Cell Death Discovery

https://doi.org/10.1038/s41420-026-03027-9

Article in Press

ADA2-deficient cells exhibit increased levels of cell death and metabolic disturbances

Received: 2 August 2025

Revised: 29 January 2026

Accepted: 5 March 2026

Cite this article as: Ehlers, L., Wouters, M., Pillay, B. *et al.* ADA2-deficient cells exhibit increased levels of cell death and metabolic disturbances. *Cell Death Discov.* (2026). https://doi.org/10.1038/s41420-026-03027-9

Lisa Ehlers, Marjon Wouters, Bethany Pillay, Selket Delafontaine, Giorgia Bucciol, Marco Baggio, Mariia Dzhus, Anneleen Hombrouck, Alexandra Damerau, Lien De Somer, Rik Schrijvers, Steven Vanderschueren, Maarten Jacquemyn, Tilmann Kallinich, Dirk Daelemans, Bart Ghesquière, Patrizia Agostinis, Leen Moens & Isabelle Meyts

ADA2-deficient cells exhibit increased levels of cell death and metabolic disturbances

Running title: Cell death in deficiency of adenosine deaminase 2

Lisa Ehlers, MD, PhD[1,2,3,4,5], Marjon Wouters, PhD[1], Bethany Pillay, PhD[1], Selket Delafontaine, MD, PhD[1,6], Giorgia Bucciol, MD, PhD[1,6], Marco Baggio, PhD[1,7], Mariia Dzhus, MD[1], Anneleen Hombrouck, PhD[1], Alexandra Damerau, PhD[5,8], Lien De Somer, MD, PhD[6,9], Rik Schrijvers, MD, PhD[10], Steven Vanderschueren, MD, PhD[11,12,13], Maarten Jacquemyn[14], Tilmann Kallinich, MD[2,3,4,5], Dirk Daelemans, PhD[14], Bart Ghesquière, PhD[15], Patrizia Agostinis, PhD[16], Leen Moens, PhD[1], Isabelle Meyts, MD, PhD[1,6]

Affiliations:

1 Department of Microbiology, Immunology and Transplantation, Laboratory for Inborn Errors of Immunity, KU Leuven, Leuven, Belgium

2 Department of Pediatric Respiratory Medicine, Immunology and Critical Care Medicine, Charité – Universitätsmedizin Berlin, corporate member of Freie Universität Berlin and Humboldt-Universität zu Berlin, Berlin, Germany

3 Berlin Institute of Health at Charité – Universitätsmedizin Berlin, Berlin, Germany

4 German Center for Child and Adolescent Health (DZKJ), partner site Berlin, Berlin, Germany

5 Deutsches Rheuma-Forschungszentrum, an Institute of the Leibniz Association, Berlin, Germany

6 Department of Pediatrics, University Hospitals Leuven, Leuven, Belgium

7 Laboratory of Computational and Developmental Biology, Berlin Institute for Medical Systems Biology (BIMSB), Max-Delbrück-Centrum for Molecular Medicine in the Helmholtz Association (MDC), Berlin, Germany

8 Charité – Universitätsmedizin Berlin, corporate member of Freie Universität Berlin and Humboldt-Universität zu Berlin, Department of Rheumatology and Clinical Immunology, Berlin, Germany

9 Laboratory of Immunobiology, Department of Microbiology and Immunology, KU Leuven, Leuven, Belgium

10 Department of Microbiology, Immunology and Transplantation, Allergy and Clinical immunology Research group, KU Leuven, Leuven, Belgium

11 Department of General Internal Medicine, University Hospitals Leuven, Leuven, Belgium

12 Department of Microbiology, Immunology and Transplantation, KU Leuven, Leuven, Belgium

13 European Reference Network for Immunodeficiency, Autoinflammatory, Autoimmune and Pediatric Rheumatic disease (ERN-RITA)

14 KU Leuven Department of Microbiology, Immunology and Transplantation, Molecular Genetics and Therapeutics in Virology and Oncology Research Group, Rega Institute for Medical Research, Leuven, Belgium

15 Department of Cellular and Molecular Medicine, Laboratory of Applied Mass Spectrometry, KU Leuven, Leuven, Belgium

16 Cell Death Research & Therapy (CDRT) Lab, Department of Cellular & Molecular Medicine, Center for Cancer Biology, VIB-KU Leuven, Leuven, Belgium

Corresponding author:

Isabelle Meyts, Laboratory for Inborn Errors of Immunity and Department of Pediatrics UZ Leuven, Herestraat 49, 3000 Leuven, Belgium; Tel +32 16 343841; Fax +32 16 343842; isabelle.meyts@uzleuven.be

Competing Interests statement:

The authors have no financial interests to declare. LE and IM have a patent application in the field of DADA2 research but not directly related to this work (PCT/EP2024/078038). The rest of the authors declare that they have no relevant conflicts of interest.

Abstract

Deficiency of adenosine deaminase 2 (DADA2) causes a complex phenotype of autoinflammation and immunodeficiency. Bone marrow failure is often refractory to treatment with tumour necrosis factor-alpha (TNF-alpha) inhibitors and additional treatment options are needed. However, the pathomechanisms underlying the disease remain incompletely understood.

The aim of this study was to examine the viability and metabolic profile of ADA2-deficient cells and to characterize the activity of different cell death pathways to advance the mechanistic understanding of DADA2.

By flow cytometry and western blot, we showed that ADA2$^{-/-}$ U-937 cells and PBMCs from DADA2 patients showed significantly elevated levels of cell death compared with cells expressing wild-type *ADA2*. Viability of ADA2-deficient cells was not improved by inhibitors of apoptosis, necroptosis, pyroptosis and ferroptosis. Blocking of TNF-alpha, type I interferon and STING signalling as well as reintroduction of wild-type ADA2 protein did not rescue the cell death phenotype *in vitro*. ADA2-deficient cells had an aberrant morphology with increased cell size and granularity and were impaired in their proliferative capacity. To identify the cause of the impaired viability, we performed ^{13}C glucose tracer metabolomics experiments which revealed disturbances in the pentose phosphate pathway of ADA2-deficient cells. This tended to be associated with increased exposure to intracellular reactive oxygen species that was attenuated in the PBMCs of a DADA2 patient measured after successful hematopoietic stem cell transplantation.

Collectively, our findings established increased levels of cell death as a possible pathomechanism of DADA2 and showed that the absence of ADA2 leads to an impairment of the pentose phosphate pathway which may account for the cellular vulnerability of ADA2-deficient cells.

Introduction

Deficiency of adenosine deaminase 2 (DADA2) is an inborn error of immunity that manifests with a complex phenotype of inflammation, vasculitis, immunodeficiency and bone marrow failure.[1] Biallelic mutations in the *ADA2* gene lead to impaired secretion of the ADA2 protein and absent ADA2 enzyme activity in the serum of DADA2 patients.[2,3] Immunologically, patients have been described to have an elevated type I and type II interferon signature and the inflammatory phenotype is often responsive to treatment with tumour necrosis factor-alpha inhibitors (TNFi).[4,5] DADA2 patients presenting with bone marrow failure often require hematopoietic stem cell transplantation and disease lethality is 8%.[6] Despite the increasing number of reported patients and studies characterizing large numbers of pathogenic variants,[7,8] genotype-phenotype correlations are difficult to establish and the pathomechanisms driving the disease remain elusive.[9,10] As a consequence, new treatment targets have hardly been identified since the initial description of the disease. Consequently, a better grasp of the pathways driving the disease is urgently needed.

Early studies into the mechanisms underlying DADA2 mentioned the increased propensity of ADA2-deficient cells for cell death or membrane instability.[2,11] Regulated cell death has been established as a driver of inflammation and damage or danger signal, and cytokines can in turn induce inflammatory forms of cell death.[12]

Therefore, we analyse levels and different forms of cell death in primary human immune cells from healthy controls (HC) and DADA2 patients and ADA2-deficient U-937 cells and describe the metabolic profile of DADA2 patients.

Results

Peripheral blood mononuclear cells from DADA2 patients show increased levels of basal cell death but reduced induction of necroptosis *in vitro*

We isolated mononuclear cells (PBMCs) from the peripheral blood of ten DADA2 patients (**Supplementary Table S1**) and analysed their viability compared with PBMCs from healthy donors. Loss of viability was determined by flow cytometry after 5-hour monoculture of isolated CD14+ monocytes. We found that baseline levels of cell death were significantly higher in the DADA2 patients' cells (7.59 ± 1.11% [mean ± standard error of the mean] compared with healthy controls (HC) (3.87 ± 0.43%). In two pairs of siblings with identical genotypes but different clinical phenotypes, the severity of their clinical symptoms correlated with the levels of cell death at baseline (**Figure 1A**). To further elucidate the relationship between the clinical phenotype and cell death, we characterised our cohort with respect to the patients' predominant phenotype as defined in the DADA2 management guidelines.[13] For patients with ample clinical information, the DADA2 disease activity index (DADA2AI) was determined.[14] **Figure 1B** shows the leading symptoms of the respective disease phenotypes reflected within the DADA2AI. In a subcohort of our patients, cell death levels in CD14+ monocytes weakly correlated with disease activity ($r = 0.5$, $p = 0.14$) (**Figure 1C**). This tendency was not observed when evaluating whole blood interferon scores ($r = -0.1$, $p = 0.73$) (**Figure 1C**). We did however find a higher interferon signature in DADA2 patients with an inflammatory phenotype compared with those with predominant bone marrow failure irrespective of disease activity (**Figure 1C**).

In addition, we analysed levels of cyclophilin A in the urine of our patients compared to paediatric healthy controls as a marker of necroptotic cell death.[15] Here, we did not observe an increase in cyclophilin A (**Supplementary Figure S1**). Urine samples were however collected in the flare-free interval in all patients.

We hypothesized that the difference in cellular viability was due to a higher baseline activation of inflammatory pathways in DADA2 which could further sensitize these immune cells to regulated cell death (RCD). To test this hypothesis, we induced necroptosis as well as apoptosis *in vitro* in HC and DADA2 monocytes as RCD paradigms with opposite inflammatory outputs. The Smac mimetic (SM) birinapant promotes degradation of cellular inhibitor of apoptosis proteins (cIAPs), thereby inducing apoptosis upon stimulation with TNF-alpha *in vitro*. Simultaneous inhibition of caspases by Z-VAD-FMK (Z-VAD) blocks apoptosis and causes necroptotic cell death (**Figure 2A**). While exhibiting elevated levels of cell death at baseline, CD14+ monocytes of DADA2 patients did not show increased levels of apoptosis or necroptosis upon *in vitro* induction of inflammatory cell death (**Figure 2B**). Of note, we found that there was reduced induction of necroptosis when measured by fold-change to baseline levels of cell death (**Figure 2B**). Induction of apoptosis was also weaker in ADA2-deficient cells although in primary monocytes the difference was not significant (**Figure 2B**). The absolute levels of cell death after necroptosis induction were however not different between HC and DADA2 cells (**Figure 2B**). No relationship was found between the cell death levels and the patients' predominant clinical phenotype (**Figure 2B**).

Both the increase in baseline cell death and the attenuated necroptosis induction were confirmed in ADA2$^{-/-}$ U-937 cell lines (**Figure 3A**). Apoptosis and necroptosis induction were verified by cleavage of caspase-3 and phosphorylation of mixed lineage kinase domain like pseudokinase (MLKL) and receptor-interacting serine/threonine-protein kinase 1 (RIPK1) on western blot (**Figure 3B, Supplementary Figure S2B+C**). In line with our findings, we showed reduced levels of phosphorylated MLKL in ADA2$^{-/-}$ U-937 cells after induction of necroptosis *in vitro* compared with cells expressing wild-type ADA2 (**Figure 3B**). Levels of total MLKL were lower both at baseline and after necroptosis induction (**Figure 3B**). No cleavage of caspase-3 was observed upon necroptosis induction.

To determine whether the increase in cell death levels in DADA2 patients' cells persisted outside the context of the inflammatory milieu present *in vivo*, we analysed cell death after increasing incubation times *in vitro*. These experiments were performed in lymphocytes because of their longer lifespan in culture. After 48 hours, CD4+ T cells showed significantly increased levels of cell death in DADA2 compared to HC. A tendency was also observed in CD8+ and CD19+ lymphocytes (**Figure 3C**). Again, patients with the highest levels of cell death showed varying phenotypes (**Figure 3C**).

In summary, we showed that PBMCs from DADA2 patients as well as ADA2$^{-/-}$ U-937 cells exhibit elevated levels of cell death at baseline but a restrained response to apoptosis and necroptosis induction *in vitro*. This phenotype tended to correlate with disease activity but was independent of the leading disease phenotype.

Increased levels of cell death in DADA2 are not rescued by inhibitors of regulated cell death

We then sought to evaluate whether the increased levels of spontaneous cell death of DADA2 cells were due to a baseline activation of RCD pathways. We therefore incubated control and ADA2-deficient cells with inhibitors of apoptosis (Z-VAD, pan-caspase inhibitor), necroptosis (necrostatin-1s, inhibitor of RIPK1) and pyroptosis (Z-YVAD, inhibitor of caspase-1) (**Figure 2A**). Efficacy of the inhibitors was confirmed by successful suppression of apoptosis and necroptosis induction as shown by western blot (**Figure 3B, Supplementary Figure S2B+C**). The inhibitors did not improve viability of DADA2 CD14+ monocytes (**Figure 4A**). These findings were confirmed after 48-hour incubation of ADA2-deficient U-937 cells as well as primary lymphocytes with the RCD inhibitors (**Figure 4B+C**). We concluded that the increase in baseline cell death observed in ADA2-deficient cells was not due to an upregulation of apoptosis, necroptosis or pyroptosis. Ferroptosis is another form of RCD driven by iron-mediated lipid peroxidation linked to inflammation.[16] Elevated levels of

cell death in lymphocytes from DADA2 patients also persisted after 48-hour incubation with the ferroptosis inhibitors deferoxamine (DFO) and ferrostatin-1 (Fer-1) (**Figure 4D**).

In conclusion, we showed that inhibition of major forms of RCD pathways does not rescue the spontaneous cell death phenotype of ADA2-deficient cells.

Cell death is not induced extrinsically by the "DADA2 milieu"

As many DADA2 patients are effectively treated with TNFi, we next examined whether this treatment attenuated the cell death phenotype of ADA2-deficient cells *in vitro*. Efficacy of the TNFi adalimumab in rescuing TNF-alpha induced cell death *in vitro* was verified by flow cytometry (**Supplementary Figure S2A**). Incubation with adalimumab over 48 hours did not affect the levels of cell death in ADA2-deficient U-937 cells or DADA2 lymphocytes (**Figure 5A+B**). As DADA2 cells exhibit an increased type I interferon signature (**Figure 5C**) and type I interferons have been shown to induce PANoptosis,[17] we hypothesized that inhibition of JAK1/2 signalling by ruxolitinib might attenuate cell death in DADA2. As for adalimumab, 48-hour incubation with ruxolitinib did not improve viability (**Figure 5A+B**). Based on previous findings suggesting that the inflammatory phenotype of ADA2-deficient cells is mediated by intracellular DNA-sensing through STING,[18] we also explored the effect of STING inhibition by H-151 on cell death in ADA2-deficient U-937 cells and did not find an improvement (**Figure 5A**). Efficacy of ruxolitinib and H-151 in suppressing the type I interferon response was verified *in vitro* (**Supplementary Figure S3**).

To further test the hypothesis that the increase in cell death in DADA2 is caused extrinsically by the "secretome" of ADA2-deficient cells, we collected supernatants of PBMCs from HC and DADA2 patients after 48-hour culture *in vitro*. Incubation of HC PBMCs with supernatants from DADA2 cells for another 48 hours did not cause increased levels of cell death compared with incubation with supernatant from HC PBMCs (**Figure 5D**).

Finally, lymphocytes were incubated with supernatant of HEK293T cells overexpressing WT and mutant (p.G47A) ADA2 protein – a variant exhibiting residual ADA2 secretion.[19] Extrinsic addition of functional ADA2 did not improve viability of ADA2-deficient cells (**Figure 5E**). Similarly, transducing ADA2$^{-/-}$ U-937 with WT *ADA2* did not rescue the cell death phenotype despite restoring physiological levels of ADA2 protein expression (**Figure 5F, Supplementary Figure S4**).

Collectively, our data suggest that the increased susceptibility to undergo spontaneous cell death in DADA2 is cell-intrinsic and not mediated by the inflammatory milieu of ADA2-deficient cells and cannot be rescued by inhibition of TNF-alpha, type I interferon signalling or STING signalling.

ADA2-deficient cells exhibit metabolic disturbances

Since we observed that ADA2-deficient U-937 cells show a substantially reduced cell growth *in vitro* compared with wild-type ADA2-expressing cells, we hypothesized that these cells exhibit impaired cell proliferation. By CellTrace™ Proliferation Assay, we identified a slight reduction in cell proliferation in ADA2$^{-/-}$ U-937 cells (**Figure 6A**). In the same experiment, we did however identify increased levels of cell death as the main contributor to the reduced cell growth over the observation period (**Figure 6B**). By microscopy, we observed an aberrant morphology of the ADA2$^{-/-}$ U-937 cell clones with a prominent increase in cell size (**Figure 6C**, **Supplementary Figure S5**). As cell size has been linked to changes in metabolism,[20,21] we hypothesized that metabolic disturbances contribute to the increase in spontaneous cell death in ADA2 deficiency. We performed tracer metabolomics experiments with ^{13}C-labelled glucose-containing medium in wild-type and ADA2$^{-/-}$ U-937 cells (**Figure 7A**). We found that ADA2-deficient cells showed decreased labelling of metabolites like NMP/NDP/NTPs, NAD(H), Acetyl (CoA) and UDP-GlcNAc that are built from nucleotides containing a ribose-5-phosphate group (**Figure 7A**). These findings indicate an impairment of the pentose phosphate pathway. Many of these metabolites were also significantly reduced in overall

abundance in ADA2-deficient cells (**Supplementary Figure S6**). As proof of concept, we performed another tracer metabolomics experiment in monocyte-derived macrophages from a DADA2 patient compared with a HC. DADA2 cells showed the same reduction in labelling of metabolites synthesized with ribose-5-phosphate from the pentose phosphate pathway (**Figure 7B**) and the same decrease in their overall abundance (**Supplementary Figure S7)**. To further validate our findings, we analysed previously published single-cell RNA sequencing data from monocytes of HCs and DADA2 patients.[11] In line with the results of the metabolomics experiments, there was a significant decrease in *PGD* expression in DADA2 monocytes (**Figure 8A**). *PGD* encodes 6-phosphogluconate dehydrogenase (6PGD), one of the key enzymes of the pentose phosphate pathway (**Figure 8B**). A critical function of the pentose phosphate pathway is the production of $NADPH+H^+$ for the regeneration of glutathione.[22] We therefore hypothesised that the impairment of this pathway might affect antioxidant capacity. We found that ADA2-deficient Jurkat cells showed elevated levels of reactive oxygen species (ROS) compared with the WT-expressing cell line (**Figure 8C**). Exposure to extrinsic oxidative stress by H_2O_2 attenuated these differences (**Figure 8C**). We confirmed this finding in the PBMCs of DADA2 patient P5 (**Figure 8D**). As proof of principle, we also included a sample from patient P6 that had at this point undergone successful hematopoietic stem cell transplantation (HSCT) (**Figure 8D**). Indeed, we found baseline ROS levels close to HC in the transplanted patient's PBMCs, hinting at a rescue of the metabolic phenotype upon HSCT in line with the clinical resolution of the patient's phenotype (**Figure 8D**).

Overall, we showed that ADA2-deficient cells exhibit an impairment in the pentose phosphate pathway likely leading to an impairment of the oxidative stress response that is improved by HSCT.

Discussion

In this study, we show that ADA2 deficiency is characterized by increased levels of cell death and an impairment of the pentose phosphate pathway.

The observation that ADA2-deficient cells are more prone to spontaneous cell death was already reported in the first description of the disease.[2] Additional reports remarked on the fragility of DADA2 patients' cells in culture.[11] Despite these findings, the mechanisms underlying the increased levels of cell death and its contribution to the immunological and clinical phenotype of DADA2 remained elusive. Recently, the role of inflammatory cell death in the pathogenesis of inflammatory diseases has been increasingly explored.[15,23,24] The advent of targeted therapies directed against key cytokines involved in the different cell death pathways highlights the clinical importance of identifying the leading pathways to guide treatment choices: Patients whose phenotype is driven by TNF-alpha-induced necroptotic cell death may benefit from TNFi, and interleukin-1 inhibitors have markedly improved the outcome of patients with autoinflammatory diseases driven by increased pyroptosis.[23,25] Especially DADA2 patients whose predominant clinical phenotype is vasculitis clinically benefit from treatment with TNFi. We therefore suspected an involvement of necroptosis in the inflammatory phenotype of the disease. While our data confirm that elevated levels of baseline cell death are a characteristic of ADA2-deficient cells, the phenotype is unresponsive to inhibitors of the necroptotic pathway. Our findings suggest that cell death in DADA2 is not driven by an RCD pathway (i.e. apoptosis, necroptosis, pyroptosis or ferroptosis). On the contrary, the elevated baseline levels of cell death appear to impair the ability of ADA2-deficient cells to undergo necroptosis (**Figure 2+3**). Cells expressing pathogenic variants of *ADA2* have been reported to exhibit an increased ER stress response.[7] A severe ER stress response is classically associated with an increase in apoptosis.[26] In our experiments, the cell death phenotype of ADA2-deficient cells did not resolve upon pharmaceutical inhibition of apoptosis.

Importantly, *in vitro* treatment with TNFi did not attenuate the cell death phenotype. TNFi have previously been shown to rescue some of the immunological phenotype of ADA2-deficient immune cells.[5] All patients included in our study were on treatment with TNFi. The cell death phenotype was present regardless of the ongoing immunomodulatory therapy, suggesting that aberrant TNF signalling is not the cause of cell death in DADA2. Similarly, Janus kinase and STING inhibitors did not rescue the phenotype, indicating that increased type I interferon and STING-signalling are not sufficient to cause increased cell death in isolation. Taking these findings into account, we conclude that inhibition of inflammation does not prevent cell death in ADA2-deficient cells and hypothesize that the two phenotypes may emerge independently. Likewise, we also analysed cell death considering the patients' predominant disease phenotypes. Consistent with the inhibitor experiments, we did not observe increased cell death in PBMCs of patients with an inflammatory/vasculitic phenotype compared with those with predominant bone marrow failure. Overall, disease phenotypes were distributed equally across samples with more or less prominent cell death levels. However, we found that disease severity tended to correlate with the severity of the cell death phenotype. This was particularly evident in two pairs of siblings with diverging disease severity and corresponding cell death levels. Our attempt to objectify this finding using the DADA2AI only showed a mild association. This is likely due to the small sample size and the fact that the activity index was designed with the predominant goal to capture disease activity in patients over time, noting improvement or worsening of symptoms.[14] Its design is therefore not ideal for the inter-patient comparison performed in this study. Our data do however suggest that the cellular mechanisms that enhance cell death in ADA2-deficient cells contribute to the severity of the clinical phenotype.

DADA2 patients with a predominant phenotype of bone marrow failure are often unresponsive to treatment with TNFi and the pathomechanism driving cytopenia in DADA2 is not yet understood.[6] Our results indicate that – independently of TNF-alpha signalling – increased cell death may

contribute to bone marrow failure in DADA2. At present, DADA2 patients with treatment-refractory cytopenia often require HSCT and additional therapeutic options are needed. Identifying the causes of cell death in DADA2 will be crucial to improve the treatment of these patients.

ADA2 was initially characterized as a secreted homodimeric enzyme that mediates adenosine deamination in the extracellular space. Due to its weak affinity to adenosine and the superior catalytic activity of its isoenzyme ADA1, recent research has suggested an intracellular deaminase-independent function of ADA2.[18,27,28] Since the cell death phenotype was not reproduced in HC PBMCs by medium transfer from DADA2 cells, our data indicate that the mechanisms that affect viability of ADA2-deficient cells are cell-intrinsic. A limitation to this experiment is that the supernatants from DADA2 cells likely do not perfectly mimic the extracellular environment found *in vivo*. In addition, the cell death phenotype was not rescued by reintroducing ADA2 to ADA2-deficient cells *in vitro*. This could indicate that cells exhibit long-term homeostatic dysregulation, e.g. due to epigenetic changes, induced by the prior absence of ADA2. It is therefore likely that ADA2 deficiency causes increased cell death via an indirect route that is not immediately fixed by adding functional ADA2. Considering the uncertainty regarding the physiologically relevant cellular function of ADA2,[10] we will need more in depth studies to identify the mechanistic relationship between absence of ADA2 and cellular disturbances. The proposed indirect mechanism is in line with the fact that increased senescence has also been observed in mesenchymal stromal cells of DADA2 patients – cells with minimal endogenous ADA2 protein expression.[29]

Until now, the focus of DADA2 research has been on the inflammatory processes underlying the disease.[2,11,30] By identifying increased cell death as a feature of DADA2, we describe an additional mechanism that is according to our data not directly linked to the inflammatory signature. By microscopy, we observed striking differences in the cell morphology of ADA2-deficient cells. We therefore assumed that ADA2 deficiency affects pathways involved in cell structure and metabolism.

The traditional function of ADA2 as a deaminase is in the purine metabolism.[31] We therefore performed tracer metabolomics experiments and identified an impairment in the pentose phosphate pathway in the absence of ADA2. Expression of *PGD* is downregulated in DADA2 monocytes (**Figure 8A**), possibly accounting for the metabolic impairment we observed. Suppression of *PGD* has been found to cause ER stress and impaired protein secretion – both cellular characteristics of DADA2.[3,7,32] It is therefore possible that the decrease in 6-phosphogluconate dehydrogenase links different aspects of the pathophysiology of ADA2-deficient cells. Further work will be needed to understand how ADA2 deficiency affects *PGD* expression. Adenosine – the substrate of ADA2 activity – contains a ribose group that is supplied by the pentose phosphate pathway. Nucleotides and nucleosides including adenosine have diverse cellular functions ranging from DNA building blocks over energy supply to signal transmitters. At the same time the pentose phosphate pathway is involved in cellular homeostasis by providing $NADPH+H^+$ for glutathione regeneration (**Figure 8B**).[22] Thus, a dysfunction of the pentose phosphate pathway is likely to disrupt multiple cellular functions and cause a diverse cellular phenotype, such as the one seen in DADA2. In an initial experiment, we confirmed that ADA2-deficient cells showed an increased ROS content in line with a reduced antioxidant capacity. Further studies will be needed to verify the contribution of this mechanism to the DADA2 phenotype and to evaluate its potential as a therapeutic target.

This study provides the first in-depth analysis of cell death in DADA2. The main limitation of the results presented here is that they largely convey negative findings. The study was conducted in a hypothesis-guided way. While our findings strongly indicate that cell death in DADA2 is not driven by one of the major RCD pathways, it cannot be excluded that these pathways still have a role in the pathogenesis of DADA2. RCD pathways are interconnected and difficult to analyse in isolation. It is however clear from our data that there must be additional drivers as combined specific inhibition of apoptosis, necroptosis and pyroptosis did not resolve the primary phenotype.

Our study is the first to identify a metabolic dysfunction in ADA2-deficient cells. While the mechanistic basis of the differences is yet to be understood, these findings provide the foundation to explore a new field in ADA2 research. Given the urgent need for improved treatment options, especially in DADA2 patients with bone marrow failure, this new direction could be crucial in the search for new therapeutic targets in DADA2.

In conclusion, we demonstrate increased levels of cell death in ADA2-deficient cells that are not due to regulated cell death pathways and establish an impaired pentose phosphate pathway as a potential cause of this phenotype.

Materials and methods

Human subjects and sample preparation

The patients were treated at University Hospitals Leuven and their parents were included as heterozygous carriers. Healthy donors were recruited at University Hospitals Leuven and KU Leuven. All study participants provided informed consent. A detailed description of the sample processing has been reported before and parts of the methodology described in this manuscript were previously reported by the authors in another study.[33]

Clinical phenotyping

Clinical information was recorded at the time of sampling. The patients' disease phenotype was determined guided by the leading symptoms categorised as proposed in the guidelines for the management of DADA2.[13] The DADA2 activity index DADA2AI was determined by the treating physician and documented as described by Bucciol et al.[14]

Sanger sequencing

Genomic DNA samples were prepared from heparinized peripheral blood following the instructions of the QIAamp DNA Blood Mini kit (#51104; QIAGEN, Hilden, Germany). Primers were designed with the help of Oligo Primer Analysis Software version 7 (Molecular Biology Insights, Colorado Springs, CO, USA). ADA2-specific gDNA amplification was performed using Platinum™ SuperFi™ PCR Master Mix (#12358010; Thermo Fisher Scientific, Waltham, MA, USA). PCR products were purified using the QIAquick PCR purification kit (#28106; QIAGEN). Sanger sequencing was performed on an ABI 3730 XL Genetic Analyzer (Applied Biosystems, Waltham, MA, USA) at LGC Genomics (Berlin, Germany). Sequencing data were analysed using Chromas 2.6.5 (http://www.technelysium.com.au).

Cell culture

Peripheral blood mononuclear cells (PBMCs) were isolated by density gradient centrifugation using Lymphoprep™ (#1114546; PROGEN, Heidelberg, Germany) in SepMate™ isolation tubes (#85450; STEMCELL Technologies, Vancouver, Canada) according to the manufacturer's instructions. Prior to monocyte isolation, the final centrifugation step was performed at 300xg for 10 minutes at 4°C. CD14+ monocytes were isolated magnetically by positive selection using human CD14 MicroBeads (#130-050-201; Miltenyi Biotec, Bergisch Gladbach, Germany) on LS columns (#130-042-401; Miltenyi Biotec) according to the manufacturer's protocol. The cells were eluted into complete medium (RPMI 1640 medium (#61870044; Gibco, Carlsbad, CA, USA) supplemented with 10% fetal calf serum (FCS) (#S181BH-500, Biowest, Nuaillé, France) and 1% penicillin-streptomycin (#15140122; Gibco). Purity > 97% of CD14+ monocytes after magnetic sorting was verified by flow cytometry (anti-CD14-FITC clone MφP9, 1:40, #345784; BD Biosciences). For macrophage differentiation, $3x10^5$ CD14+ monocytes were seeded in a 12-well plate in 1 mL complete medium

containing 20 ng/mL GM-CSF (#300-03; Peprotech, Rocky Hill, NJ, USA). The cells were differentiated for ten days, with medium changes every three days. U-937 cells and Jurkat cells (ATCC, Manassas, VA, USA) were cultured in complete RPMI medium.

Transfection

The plasmid expressing myc-DDK-tagged wild-type ADA2 (transcript variant 3, NM_001282225) was purchased from OriGene Technologies (#RC238645). Pathogenic *ADA2* variants were created by site-directed mutagenesis using the Q5® Site-Directed Mutagenesis Kit (#E0554; New England Biolabs) according to the manufacturer's instructions. Stable competent E. coli (#C3040H, New England Biolabs) were transformed with the generated constructs. Plasmid DNA was purified with the help of the QIAprep Spin Miniprep Kit (#27104, QIAGEN). Successful mutagenesis was verified by Sanger sequencing (LGC Genomics). HEK293T cells were seeded at $2.5x10^5$ cells/well in 2 mL in a 6-well plate 24h prior to transfection. The cells were transfected with 1 μg plasmid DNA, using Lipofectamine™ 2000 Transfection Reagent (#11668019; Invitrogen) according to the manufacturer's instructions. The medium was changed after 24h. Supernatants were collected 72h after transfection.

Generation of ADA2$^{-/-}$ cell lines by CRISPR/Cas9

Single-guide RNAs targeting *ADA2* from the human CRISPR Brunello library (#73179; addgene, Watertown, MA, USA)[34] were cloned into the lentiCRISPRv2 puro plasmid. lentiCRISPRv2 puro was a gift from Brett Stringer (plasmid #98290; addgene; http://n2t.net/addgene:98290; RRID:Addgene_98290). U-937 cells and Jurkat cells were transfected by electroporation using the

Neon™ Transfection System (#MPK5000; Thermo Fisher Scientific) according to the manufacturer's instructions.[33]

Transduction

Pathogenic *ADA2* variants were created by site-directed mutagenesis as described above. Fragments containing the sequence coding for the untagged ADA2 protein were then generated using the following primers and CloneAmp™ HiFi PCR Premix (#639298; Takara Bio):

ORF_ADA2_PSPXI_F_GGTGGTACTCGAGTATGTTGGTGGATGGCCCATCTGA;

ORF_ADA2_PmeI_R_GGTGGTGTTTAAACCTTTGTAGCCACATCTGCTATGAACTT.

The fragments were cleaned up using the QIAquick PCR Purification Kit (#28104; QIAGEN) and cloned into the p3D lentiviral expression vector as follows: Restriction of the expression vector was performed in CutSmart buffer (#B7204; New England Biolabs) with PspX1 (#R0656; New England Biolabs) and PmeI (#R0560; New England Biolabs) at 37 °C overnight followed by 20-minute heat inactivation at 65 °C. Dephosphorylation of 5´-ends was performed using rSAP (#M0371; New England Biolabs) at 37 °C overnight followed by 20-minute heat inactivation at 65 °C. The PCR fragments were subsequently inserted into the expression vector using T4 ligase (#M0202; New England Biolabs) for 10 minutes at room temperature followed by 10-minute heat inactivation at 65 °C. After DNA cleanup (#28104; QIAGEN), stable competent E. coli (#C3040H, New England Biolabs) were transformed with the generated plasmids. Plasmid DNA was purified with the help of the QIAprep Spin Miniprep Kit (#27104, QIAGEN). Sanger sequencing (LGC Genomics) was performed to confirm that the genetic information for *ADA2* was intact and that the respective mutations were present. Lentiviral particles were generated by transfecting HEK293T cells with the plasmids p3A (Gag-Pol), p3B (Rev), p3C (VSV-G) and p3D (expression vector) at a ratio of 1:1:1:3 using Lipofectamine™ 2000 Transfection Reagent (#11668019; Invitrogen). Supernatants containing

lentiviral particles were harvested 48h and 72h after transfection. The viral titer was determined using the qPCR Lentivirus Titer Kit (#LV900; Applied Biological Materials). Viral supernatants were prepared at MOI=40 with 8 μg/mL polybrene and 10^6 U-937 cells were transduced by spinoculation at 700xg for 2 hours at 32 °C. After 4 hours at 37 °C, the supernatant was replaced by fresh complete RPMI medium. Selection with 1 μg/mL puromycin (#ant-pr-1; InvivoGen) was started 48 hours after the transduction.

Flow cytometry

Cells were placed on ice at the end of the incubation period and washed with PBS prior to staining with the following primary antibodies: anti-CD4-APC-H7 (clone RPA-T4, 1:20, #560158; BD Biosciences, Franklin Lakes, NJ, USA; RRID: AB_1645478) anti-CD8-PE-Cy5.5 (clone RPA-T8, 1:20, #35-0088-42; Thermo Fisher Scientific; RRID: AB_11218701), anti-CD14-FITC (clone MφP9, 1:40, #345784; BD Biosciences), anti-CD19-BV421 (clone HIB19, 1:20, #302234; BioLegend, San Diego, CA, USA; RRID: AB_11142678). The viability staining was performed with the following reagents: Zombie Violet™ Fixable Viability Dye (1:1000, #423113, BioLegend) and Annexin V-APC (1:100, #550474, BD Biosciences; RRID: AB_2868885) in 1X Annexin V Binding Buffer (#556454, BD Biosciences). Prior to flow cytometric analysis, the cells were fixed in 1% formaldehyde in Annexin V Binding Buffer.

ROS content was determined with the help of the Total Reactive Oxygen Species (ROS) Assay Kit 520 nm (#88-5930-74, Thermo Fisher Scientific) used according to the manufacturer's instructions.

The measurements were performed on Canto II and Symphony flow cytometers (BD Biosciences). The data were analysed with FlowJo software (version 10.8.1). For analysis, debris was excluded by forward and sideward scatter and singlets were identified before determining the percentage of dead cells.

Cell proliferation assay

Cell proliferation was assessed by CellTrace™ Yellow Cell Proliferation Assay (#C34573; Thermo Fisher Scientific). U-937 cells were stained in CellTrace working solution at 1:500 in PBS according to the manufacturer's instructions. Samples were taken after 10 minutes (baseline) and 2, 4, and 6 days respectively. Cells were prepared for flow cytometry by additionally staining with a fixable viability dye (see above) and fixing in 2% formaldehyde in PBS.

Cell death assay

Cells were seeded in a 24-well plate at $2.5x10^5$ cells in 500 µL complete medium. Prior to induction of cell death, the cells were incubated for 30 minutes with inhibitors of different forms of regulated cell death as indicated: 20 µM Z-VAD-FMK (#S7023; Selleck Chemicals GmbH, Houston, TX, USA), 20 µM Z-DEVD-FMK (S7312; Selleck Chemicals GmbH), 10 µM necrostatin-1s (#S8641; Selleck Chemicals GmbH), 1 µM necrosulfonamide (#S8251; Selleck Chemicals GmbH), 20 µM Z-YVAD-FMK (#S8507; Selleck Chemicals GmbH), 50 µM deferoxamine (#S5742; Selleck Chemicals GmbH), 2 µM ferrostatin-1 (#S7243; Selleck Chemicals GmbH).

Apoptosis was induced by 30-minute incubation with 100 nM birinapant (#S7015; Selleck Chemicals GmbH) followed by 4-hour incubation with 20 ng/mL TNF-α (#rcyc-htnfa; InvivoGen, San Diego, CA, USA). Necroptosis was induced by 30-minute incubation with 100 nM birinapant (#S7015; Selleck Chemicals GmbH) and 20 µM Z-VAD-FMK (#S7023; Selleck Chemicals GmbH) followed by 4-hour incubation with 20 ng/mL TNF-α (#rcyc-htnfa; InvivoGen).

TNF inhibition was achieved by incubation with 5 µg/mL adalimumab (#A2010, Selleck Chemicals GmbH). Ruxolitinib (5 µM, #S1378, Selleck Chemicals GmbH) was used to block JAK1/2 signalling

and the STING-inhibitor H-151 (1 μM, #inh-h151, InvivoGen) served to examine DNA sensing. Effective concentrations were determined by titration after stimulation of the respective pathways (**Supplementary Figure S2A+B** and **S3**).

Immunoblotting

Whole cell lysates were obtained by lysing $1x10^6$ cells in 25 μL RIPA buffer (150 mM NaCl, 1% Triton X-100, 0.5% sodium deoxycholate, 0.1% SDS, pH 8.0) containing protease inhibitor (#78429; Thermo Fisher Scientific) for 30 minutes on ice, followed by centrifugation at 13,500xg for 20 minutes at 4°C. Bolt™ LDS sample buffer (#B0007; Thermo Fisher Scientific) mixed with Bolt™ Sample Reducing Agent (#B0009; Thermo Fisher Scientific) was added to the samples prior to gel electrophoresis. 1200 μL ice-cold acetone were added to 300 μL urine and the samples were inverted and vortexed thoroughly for protein precipitation. After overnight incubation at -20°C, the samples were spun for 15 minutes at 15,000xg at 4°C. Supernatants were discarded, pellets resuspended in 75 μL 1X sample buffer and placed at 95°C for 10 minutes. 20 μL were loaded onto the gel. SeeBlue™ Plus2 Pre-stained Protein Standard (#LC5925; Thermo Fisher Scientific) was used as protein molecular weight marker. Proteins were transferred onto PVDF transfer membranes. Ponceau S was used according to the manufacturer's instructions. The membranes were probed with the following primary antibodies: anti-ADA2 (clone EPR25430-131, #ab288296, 1:1000; abcam, Cambridge, UK), anti-pMLKL (S358) (clone: D6H3V, #91689, 1:1000; Cell Signaling Technology, Danvers, MA, USA; RRID:AB_2732034), anti-MLKL (clone: D2I6N, #14993, 1:1000; Cell Signaling Technology; RRID:AB_2721822), anti-pRIP (Ser166) (clone: D1L3S, #65746, 1:1000; Cell Signaling Technology; RRID:AB_2799693), anti-RIP (clone: D94C12, #3493, 1:1000; Cell Signaling Technology; RRID:AB_2305314), anti-cleaved caspase-3 (Asp175) (clone: 5A1E, #9664, 1:1000; Cell Signaling Technology; RRID:AB_2070042), anti-caspase-3 (#9662, 1:1000; Cell Signaling Technology;

RRID:AB_331439), anti-cyclophilin A (#ab41684, 1:1000; abcam; RRID:AB_879768), anti-GAPDH (clone: 7B, #sc-69778, 1:500; Santa Cruz Biotechnology, Dallas, TX, USA; RRID:AB_1124759), and anti-β-actin (clone: AC-15, #A5441, 1:9,000; Sigma-Aldrich, St. Louis, MO, USA; RRID: AB_476744) at 4°C overnight or at room temperature for two hours. The membranes were washed and incubated with the respective HRP-coupled secondary antibodies for one hour at room temperature: goat anti-rabbit IgG H&L (#ab205718, 1:5000; abcam; RRID: AB_2819160) or Goat Anti-Mouse IgG (H + L) (#71045, 1:5000; Sigma-Aldrich; RRID: AB_11211441). Protein expression was visualized by enzymatic chemiluminescence using Pierce™ ECL western blotting substrate (#32106; Thermo Fisher Scientific) or SuperSignal™ West Pico PLUS Chemiluminescent Substrate (#34580; Thermo Fisher Scientific) in a ChemiDoc XRS+ Imaging System (Bio-Rad). Protein bands were quantified with the help of Image J. The full length uncropped western blots are provided in the Supplementary Material.

Microscopy

U-937 cells were cultured in complete RPMI medium. The immunofluorescence staining was performed in V-shaped 96-well plates in the dark at room temperature (RT). Cells were harvested, fixed in 4% (v/v) paraformaldehyde (Electron Microscopy Sciences) for 10 minutes, and permeabilized with PBS containing 0.1% Tween®20 (Qbiogene Inc.) for 10 minutes. To prevent nonspecific antibody binding, cells were incubated in blocking buffer (1x PBS supplemented with 5% FCS and 5 mg/mL human IgG; IgG1 66.6%, IgG2 28.5%, IgG3 2.7%, IgG4 2.2%; Grifols) for 30 minutes. Nuclear staining was performed using DAPI (1 μg/mL in PBS / 0.1% Tween®20) for 15 minutes. For imaging, stained cells were transferred onto glass slides using a Cytospin 4 centrifuge (Thermo Fisher Scientific) at 800 rpm for 3 minutes with medium acceleration. Images were acquired with a laser scanning confocal fluorescence microscope (LSM 710, Carl Zeiss).

In addition, cell morphology was evaluated in the culture plate by brightfield microscopy on an EVOS M7000 Microscope Imaging System (#AMF7000; Invitrogen, Waltham, MA, USA) using the 20x objective.

qPCR

5-10x10^5 cells were lysed in TRIzol™ Reagent (#15596018; Thermo Fisher Scientific) for 3 minutes at room temperature and homogenized before storage at -80°C. RNA was extracted using the PureLink™ RNA Mini Kit (#12183018A; Thermo Fisher Scientific) according to the manufacturer's instructions. cDNA was generated from 20 ng RNA using the SuperScript™ VILO™ cDNA Synthesis Kit (#11754050; Thermo Fisher Scientific). Quantitative polymerase chain reaction (qPCR) analysis was performed with SsoAdvanced™ Universal SYBR® Green Supermix (#1725271; Bio-Rad Laboratories, Hercules, CA, USA) and the following primers:

IFI27_F_TCGCCTCGTCCTCCATAGCAG;

IFI27_R_ AGTAGAACCTCGCAATGACAGCC;

IFI44L_F_ATCTTAAAAGGTTGTATGCCAGA;

IFI44L_R_ACTTGCTTCACTTTTGCCAA; IFIT1_F_ATGAGTACAAATGGTGATGA;

IFIT1_R_AATTCAATCTGATCCAAGAC; ISG15_F_GGTGGACAAATGCGACGAACCTC;

ISG15_R_CACACCCTCCAGCCCGCTCA; RSAD2_F_ GCGTCAACTATCACTTCACTCG;

RSAD2_R_ CAGGTATTCTCCCCGGTCT; SIGLEC1_F_ TCTTGCCCAAGCTTCTCCTC;

SIGLEC1_R_GTAGTACCAGATGGCCGTGA;

GAPDH_F_GTCTCCTCTGACTTCAACAGCG;

GAPDH_R_ACCACCCTGTTGCTGTAGCCAA. For all conditions, three technical replicates were measured. The experiment was run on a QuantStudio™ 3 Real-Time PCR System (Thermo Fisher Scientific) and analysed using the QuantStudio™ Design & Analysis Software v1.5.2. The relative

abundance of the respective gene was normalized to the expression level of *HPRT1* or *GAPDH*. and different conditions were compared using the $2^{-\Delta\Delta Ct}$ method.[35]

For analysis of whole blood samples, total RNA was extracted from PAXgene RNA tubes using the PAXgene Blood RNA Kit, v2 (PreAnalytiX, Qiagen/ BD). The median fold change of the six interferon-stimulated genes *IFI27*, *IFI44L*, *IFIT1*, *ISG15*, *RSAD2*, *SIGLEC1* when compared to expression in healthy control samples was used to create an interferon score for each individual.[36]

Metabolomics

Magnetically sorted CD14+ monocytes from healthy control and DADA2 patients were seeded at $3x10^5$ cell/well in 2 mL complete RPMI medium in a 6-well plate and cultured for 10 days with 20 ng/mL GM-CSF. Medium changes were performed every three days. On day 10, the medium was replaced by RPMI medium containing ^{13}C-labelled glucose supplemented with 10% dialyzed medium (3 replicates). One well was incubated with RPMI medium containing ^{12}C glucose at the same concentration. After 24-hour incubation, the medium was removed, and the cells washed with ice-cold 0.9% NaCl solution. The cells were incubated in 300 µL ice-cold cellular extraction buffer (80% methanol containing 2 µM d27 myristic acid). The extraction mix was then centrifuged at 20.000xg for 15 minutes at 4°C and the supernatants stored for metabolomics analysis (see below). The pellet was lysed in 200 mM NaOH solution and BCA assay performed for protein quantification.

U-937 cells were seeded at $1.5x10^6$ cells/well in ^{13}C or ^{12}C glucose-containing medium. After 24-hour incubation the cells were washed in ice-cold PBS and centrifuged at 1500xg for 5 minutes. 150 µL extraction buffer (50 : 30 : 20 methanol : acetonitrile : water, containing 10 mM Tris-HCl pH 9.4) were added and the samples vortexed thoroughly and stored overnight at -80°C. The samples were then centrifuged at >12.000xg for 15 minutes at 4°C and the supernatants used for metabolomics analysis (see below). The protein pellet was used for the BCA assay as above.

10 µL of each sample were loaded into a Dionex UltiMate 3000 LC System (Thermo Fisher Scientific) equipped with a C-18 column (Acquity UPLC -HSS T3 1. 8 µm; 2.1 x 150 mm, Waters) coupled to a Q Exactive Orbitrap mass spectrometer (Thermo Scientific) operating in negative ion mode. A step gradient was carried out using solvent A (10 mM TBA and 15 mM acetic acid) and solvent B (100% methanol). The gradient started with 5% of solvent B and 95% solvent A and remained at 5% B until 2 min post injection. A linear gradient to 37% B was carried out until 7 min and increased to 41% until 14 min. Between 14 and 26 minutes the gradient increased to 95% of B and remained at 95% B for 4 minutes. At 30 min the gradient returned to 5% B. The chromatography was stopped at 40 min. The flow was kept constant at 0.25 mL/min and the column was placed at 40°C throughout the analysis. The MS operated in full scan mode (m/z range: [70.0000-1050.0000]) using a spray voltage of 4.80 kV,capillary temperature of 300°C, sheath gas at 40.0, auxiliary gas at 10.0. The AGC target was set at 3.0E+006 using a resolution of 140000, with a maximum IT fill time of 512 ms. Data collection was performed using the Xcalibur software (Thermo Fisher Scientific). The data analyses were performed by integrating the peak areas (El-Maven – Polly - Elucidata).

Statistical analysis

Statistical analysis was performed in R and GraphPad Prism. Normality testing was performed by Q-Q-plot. Where a normal distribution could be assumed, samples were compared by t-test. Otherwise, Wilcoxon signed rank test was used for differential analysis of paired samples and Mann-Whitney-U test for differential analysis of unpaired samples.

For the tracer metabolomics experiments, the raw MS data was used as input to IsoCor v2 to perform natural abundance correction.[37] The following parameters were used: resolution reference: 140000, mz reference: 200, isotopic purity of the tracer: 100%. For each metabolite and each cell line, a t-test was performed to determine differences in mean enrichment between healthy controls and patients.

Single-cell RNA sequencing data was provided by Watanabe et al. in the form of the output of the cellranger pipeline.[11] scAR was used for ambient RNA removal and scDblFinder to identify and remove doublets (default parameters).[38,39] Further quality control was performed according to the recommendations of Heumos et al.[40] DEA was carried out by first creating pseudobulks for each donor, and then using the limma-voom method with the empirical Bayes procedure.[41,42]

Supplementary information is available at *Cell Death Discovery*'s website.

References

1. Meyts I, Aksentijevich I. Deficiency of Adenosine Deaminase 2 (DADA2): Updates on the Phenotype, Genetics, Pathogenesis, and Treatment. J Clin Immunol. 2018 July;38(5):569–78.
2. Zhou Q, Yang D, Ombrello AK, Zavialov AV, Toro C, Zavialov AV, et al. Early-onset stroke and vasculopathy associated with mutations in ADA2. N Engl J Med. 2014 Mar 6;370(10):911–20.
3. Navon Elkan P, Pierce SB, Segel R, Walsh T, Barash J, Padeh S, et al. Mutant adenosine deaminase 2 in a polyarteritis nodosa vasculopathy. N Engl J Med. 2014 Mar 6;370(10):921–31.
4. Belot A, Wassmer E, Twilt M, Lega JC, Zeef LA, Oojageer A, et al. Mutations in CECR1 associated with a neutrophil signature in peripheral blood. Pediatr Rheumatol Online J. 2014;12:44.
5. Deuitch NT, Yang D, Lee PY, Yu X, Moura NS, Schnappauf O, et al. TNF-inhibition in vasculitis management in adenosine deaminase 2 deficiency (DADA2). J Allergy Clin Immunol [Internet]. 2021 Nov 12 [cited 2021 Nov 16]; Available from: https://www.sciencedirect.com/science/article/pii/S0091674921016936

6. Hashem H, Kumar AR, Müller I, Babor F, Bredius R, Dalal J, et al. Hematopoietic stem cell transplantation rescues the hematological, immunological, and vascular phenotype in DADA2. Blood. 2017 Dec 14;130(24):2682–8.
7. Chen L, Mamutova A, Kozlova A, Latysheva E, Evgeny F, Latysheva T, et al. Comparison of disease phenotypes and mechanistic insight on causal variants in patients with DADA2. J Allergy Clin Immunol [Internet]. 2023 May 5 [cited 2023 May 8]; Available from: https://www.sciencedirect.com/science/article/pii/S009167492300564X
8. Dzhus M, Ehlers L, Wouters M, Jansen K, Schrijvers R, De Somer L, et al. A Narrative Review of the Neurological Manifestations of Human Adenosine Deaminase 2 Deficiency. J Clin Immunol. 2023 Aug 7;
9. Lee PY, Kellner ES, Huang Y, Furutani E, Huang Z, Bainter W, et al. Genotype and functional correlates of disease phenotype in deficiency of adenosine deaminase 2 (DADA2). J Allergy Clin Immunol. 2020 June;145(6):1664-1672.e10.
10. Tarrant TK, Kelly SJ, Hershfield MS. Elucidating the pathogenesis of adenosine deaminase 2 deficiency: current status and unmet needs. Expert Opin Orphan Drugs. 2022 Mar 8;0(ja):null.
11. Watanabe N, Gao S, Wu Z, Batchu S, Kajigaya S, Diamond C, et al. Analysis of deficiency of adenosine deaminase 2 pathogenesis based on single-cell RNA sequencing of monocytes. J Leukoc Biol. 2021 Sept;110(3):409–24.
12. Berghe TV, Linkermann A, Jouan-Lanhouet S, Walczak H, Vandenabeele P. Regulated necrosis: the expanding network of non-apoptotic cell death pathways. Nat Rev Mol Cell Biol. 2014 Feb;15(2):135–47.
13. Lee PY, Davidson BA, Abraham RS, Alter B, Arostegui JI, Bell K, et al. Evaluation and Management of Deficiency of Adenosine Deaminase 2: An International Consensus Statement. JAMA Netw Open. 2023 May 31;6(5):e2315894.

14. Bucciol G, Ombrello AK, Chambers EP, Meyts I. Proposal for a Disease Activity Score and Disease Damage Score for ADA2 Deficiency: the DADA2AI and DADA2DI. J Clin Immunol. 2023 Dec 22;44(1):25.

15. Tao P, Sun J, Wu Z, Wang S, Wang J, Li W, et al. A dominant autoinflammatory disease caused by non-cleavable variants of RIPK1. Nature. 2020 Jan;577(7788):109–14.

16. Chen Y, Fang ZM, Yi X, Wei X, Jiang DS. The interaction between ferroptosis and inflammatory signaling pathways. Cell Death Dis. 2023 Mar 21;14(3):1–13.

17. Karki R, Lee S, Mall R, Pandian N, Wang Y, Sharma BR, et al. ZBP1-dependent inflammatory cell death, PANoptosis, and cytokine storm disrupt IFN therapeutic efficacy during coronavirus infection. Sci Immunol. 2022 May 19;0(0):eabo6294.

18. Greiner-Tollersrud OK, Boehler V, Bartok E, Krausz M, Polyzou A, Schepp J, et al. ADA2 is a lysosomal DNase regulating the type-I interferon response [Internet]. 2020 June [cited 2021 Sept 17] p. 2020.06.21.162990. Available from: https://www.biorxiv.org/content/10.1101/2020.06.21.162990v2

19. Wouters M, Ehlers L, Van Eynde W, Kars ME, Delafontaine S, Kienapfel V, et al. Dominant negative ADA2 mutations cause ADA2 deficiency in heterozygous carriers. J Exp Med. 2025 Aug 27;222(11):e20250499.

20. Cadart C, Heald R. Scaling of biosynthesis and metabolism with cell size. Mol Biol Cell. 2022 Aug 1;33(9):pe5.

21. Glazier DS. How Metabolic Rate Relates to Cell Size. Biology. 2022 July 25;11(8):1106.

22. TeSlaa T, Ralser M, Fan J, Rabinowitz JD. The pentose phosphate pathway in health and disease. Nat Metab. 2023 Aug;5(8):1275–89.

23. Taft J, Markson M, Legarda D, Patel R, Chan M, Malle L, et al. Human TBK1 deficiency leads to autoinflammation driven by TNF-induced cell death. Cell. 2021 Aug;184(17):4447-4463.e20.

24. Lalaoui N, Boyden SE, Oda H, Wood GM, Stone DL, Chau D, et al. Mutations that prevent caspase cleavage of RIPK1 cause autoinflammatory disease. Nature. 2020 Jan;577(7788):103–8.

25. Ozen S, Ben-Cherit E, Foeldvari I, Amarilyo G, Ozdogan H, Vanderschueren S, et al. Long-term efficacy and safety of canakinumab in patients with colchicine-resistant familial Mediterranean fever: results from the randomised phase III CLUSTER trial. Ann Rheum Dis. 2020 Oct;79(10):1362–9.

26. Tabas I, Ron D. Integrating the mechanisms of apoptosis induced by endoplasmic reticulum stress. Nat Cell Biol. 2011 Mar;13(3):184–90.

27. Dong L, Luo W, Maksym S, Robson SC, Zavialov AV. Adenosine deaminase 2 regulates the activation of the toll-like receptor 9 in response to nucleic acids. Front Med [Internet]. 2024 July 30 [cited 2024 Aug 15]; Available from: https://doi.org/10.1007/s11684-024-1067-5

28. Greiner-Tollersrud OK, Krausz M, Boehler V, Polyzou A, Seidl M, Spahiu A, et al. ADA2 is a lysosomal deoxyadenosine deaminase acting on DNA involved in regulating TLR9-mediated immune sensing of DNA. Cell Rep [Internet]. 2024 Nov 26 [cited 2024 Oct 24];43(11). Available from: https://www.cell.com/cell-reports/abstract/S2211-1247(24)01250-6

29. Bulté D, Barzaghi F, Mesa-Nuñez C, Rigamonti C, Basso-Ricci L, Visconti C, et al. Early bone marrow alterations in patients with adenosine deaminase 2 deficiency across disease phenotypes and severities. J Allergy Clin Immunol. 2024 Sept 14;S0091-6749(24)00945-X.

30. Wu Z, Gao S, Watanabe N, Batchu S, Kajigaya S, Diamond C, et al. Single-cell profiling of T lymphocytes in deficiency of adenosine deaminase 2. J Leukoc Biol [Internet]. [cited 2021 Nov 4];n/a(n/a). Available from: https://onlinelibrary.wiley.com/doi/abs/10.1002/JLB.5A0621-314R

31. Zavialov AV, Yu X, Spillmann D, Lauvau G, Zavialov AV. Structural basis for the growth factor activity of human adenosine deaminase ADA2. J Biol Chem. 2010 Apr 16;285(16):12367–77.

32. Li H, Ericsson M, Rabasha B, Budnik B, Chan SH, Freinkman E, et al. 6-Phosphogluconate Dehydrogenase Links Cytosolic Carbohydrate Metabolism to Protein Secretion via Modulation of Glutathione Levels. Cell Chem Biol. 2019 Sept 19;26(9):1306-1314.e5.

33. Ehlers L, Hombrouck A, Wouters M, Pillay B, Delafontaine S, Bucciol G, et al. Human ADA2 deficiency is characterized by the absence of an intracellular hypoglycosylated form of adenosine deaminase 2 [Internet]. bioRxiv; 2024 [cited 2024 Oct 23]. p. 2023.10.25.564037. Available from: https://www.biorxiv.org/content/10.1101/2023.10.25.564037v3

34. Doench JG, Fusi N, Sullender M, Hegde M, Vaimberg EW, Donovan KF, et al. Optimized sgRNA design to maximize activity and minimize off-target effects of CRISPR-Cas9. Nat Biotechnol. 2016 Feb;34(2):184–91.

35. Livak KJ, Schmittgen TD. Analysis of relative gene expression data using real-time quantitative PCR and the 2(-Delta Delta C(T)) Method. Methods San Diego Calif. 2001 Dec;25(4):402–8.

36. Rice GI, Melki I, Frémond ML, Briggs TA, Rodero MP, Kitabayashi N, et al. Assessment of Type I Interferon Signaling in Pediatric Inflammatory Disease. J Clin Immunol. 2017 Feb 1;37(2):123–32.

37. Millard P, Delépine B, Guionnet M, Heuillet M, Bellvert F, Létisse F. IsoCor: isotope correction for high-resolution MS labeling experiments. Bioinforma Oxf Engl. 2019 Nov 1;35(21):4484–7.

38. Sheng C, Lopes R, Li G, Schuierer S, Waldt A, Cuttat R, et al. Probabilistic machine learning ensures accurate ambient denoising in droplet-based single-cell omics [Internet]. bioRxiv; 2022 [cited 2024 July 14]. p. 2022.01.14.476312. Available from: https://www.biorxiv.org/content/10.1101/2022.01.14.476312v4

39. Germain PL, Lun A, Garcia Meixide C, Macnair W, Robinson MD. Doublet identification in single-cell sequencing data using scDblFinder. F1000Research. 2022 May 16;10:979.

40. Heumos L, Schaar AC, Lance C, Litinetskaya A, Drost F, Zappia L, et al. Best practices for single-cell analysis across modalities. Nat Rev Genet. 2023 Aug;24(8):550–72.
41. Law CW, Chen Y, Shi W, Smyth GK. voom: Precision weights unlock linear model analysis tools for RNA-seq read counts. Genome Biol. 2014 Feb 3;15(2):R29.
42. Phipson B, Lee S, Majewski IJ, Alexander WS, Smyth GK. ROBUST HYPERPARAMETER ESTIMATION PROTECTS AGAINST HYPERVARIABLE GENES AND IMPROVES POWER TO DETECT DIFFERENTIAL EXPRESSION. Ann Appl Stat. 2016 June;10(2):946–63.

Acknowledgements

First, we would like to express our gratitude to our patients and their parents for their willingness to participate in our study and to their treating physicians and nurses for their efforts in the collection of research samples. Besides, we thank Lotte Bral for her assistance in the production of the knock-out cell lines.

Conflict of Interest Statement

The authors have no financial interests to declare. LE and IM have a patent application in the field of DADA2 research but not directly related to this work (PCT/EP2024/078038). The rest of the authors declare that they have no relevant conflicts of interest.

Author Contribution Statement

LE, LM, PA and IM were responsible for the study conception and design. Material preparation and data collection was performed by LE, AH, MW, BP, SD, MD, AD and LM. LE, AH, MB and LM performed the data analysis. MJ and DD assisted in the generation of ADA2 knock-out cell lines. LE, SD, GB, LDS, RS, SV, TK and IM collected clinical data and biological materials from patients. BG supported the design and performance of the metabolomics experiments and analyses. The first draft of the manuscript was written by LE. All authors reviewed the manuscript and approved its submission. IM is responsible for the supervision of the study.

Ethics Statement

This study was performed in accordance with the ethical standards as laid down in the 1964 Declaration of Helsinki and its later amendments and was approved by the Ethics Committee for Research of Leuven University Hospitals (project numbers S63077, S63807). All study participants provided informed consent.

Funding Statement

This project has received funding from the European Research Council (ERC) under the European Union's Horizon 2020 research and innovation program (GA No. 948959) (MORE2ADA2). IM is a Senior Clinical Investigator at the Research Foundation–Flanders, and is supported by a KU Leuven C1 Grant [grant number C16/18/007]; by the Research Foundation-Flanders (FWO) [grant number G0B5120N]; and by the Jeffrey Modell Foundation. This work was supported by ERN-RITA. LE was supported by a PhD Fellowship from the Research Foundation – Flanders (FWO) (grant 11E0123N).

LE is a fellow of the BIH Charité Junior Clinician Scientist Program funded by the Charité – Universitätsmedizin Berlin, and the Berlin Institute of Health at Charité (BIH). SD was supported by a PhD Fellowship from the Research Foundation – Flanders (FWO) (grant 11F4421N). AD is currently funded by the DFG (Deutsche Forschungsgemeinschaft - Project number 530960394). RS is a FWO senior clinical investigator fellow (1805523N). PA is supported by grants from the Flemish Research Foundation (FWO-Vlaanderen G0A3320N), the KU Leuven C14/21/095 InterAction consortium, the EOS MetaNiche consortium N° 40007532, the iBOF/21/053 ATLANTIS network and by the EOS DECODE consortium N° 30837538.

Data Availability Statement

The authors provide a supplementary file containing the original uncropped blots of all the presented data. Further information is available upon request.

Figure legends

Figure 1: Phenotype and cell death levels in DADA2 patients. (A) Cell death of healthy control (HC) and DADA2 (P) CD14+ monocytes was measured after 5-hour incubation *in vitro* by flow cytometry. Dead cells were identified by staining with Annexin V and Zombie® viability dye. The bottom part of the figure depicts the clinical phenotype of the patients at the time of sampling. Patients P1 and P2 as well as P5 and P6 are siblings. (B) Symptoms captured by the DADA2 activity index (DADA2AI) are displayed assigned to the corresponding disease phenotype.[13,14] Below, the predominant phenotype of the included patients is indicated by colour (red = inflammatory / vasculitic, yellow = hematologic, blue = immunodeficient). Detailed information is provided in **Supplementary Table S1**. (C) Correlation of type I interferon signature in whole blood (*left panel*) or disease activity measured by DADA2AI (*right panel*) with cell death levels of CD14+ monocytes from healthy controls (HC) and DADA2 patients measured by flow cytometric measurement of staining with Annexin V and Zombie® viability dye. The interferon score was determined by qPCR as described by Rice et al.[36] The green band indicates the normal reference range.

Figure 2: Analysis of cell death in DADA2 at baseline and after induction of apoptosis and necroptosis *in vitro*. (A) Schematic overview of the induction and inhibition of different regulated cell death pathways *in vitro*. (B) Cell death in CD14+ monocytes from healthy controls (HC) and DADA2 patients was measured by flow cytometric measurement of staining with Annexin V and Zombie® viability dye. Cells were incubated for 5 hours. Apoptosis (TS) and necroptosis (TSZ) were induced by stimulation with 100 nM birinapant (SM) ± 20 μM Z-VAD-FMK (Z-VAD) followed by 20 ng/mL tumour necrosis factor-alpha (TNF-α). Inhibition of necroptosis was achieved by adding 10 μM necrostatin-1s (Nec-1s, TSZN). Plots show median and 25th and 75th percentiles. Data from n = 19 (HC) and n = 14 (DADA2, comprising n = 7 distinct patients) independent experiments are

shown. Mann-Whitney-U test, **p < 0.01. The patients' phenotype is indicated by colour as displayed in **Figure 1B**.

Legend: cIAPs, cellular inhibitor of apoptosis proteins; DFO, deferoxamine; Fer-1, ferrostatin-1; GSDMD, gasdermin D; IL-1β, interleukin-1beta; MLKL, mixed lineage kinase domain like pseudokinase; Nec-1s, necrostatin-1s; NSA, necrosulfonamide; RIPK1, receptor-interacting serine/threonine-protein kinase 1; RIPK3, receptor-interacting serine/threonine-protein kinase 3; SM, Smac mimetic; TRADD, tumour necrosis factor receptor type 1-associated DEATH domain protein; TRAF2, TNF receptor-associated factor 2; Z-VAD, Z-VAD-FMK; Z-YVAD, Z-YVAD-FMK.

Figure 3: Analysis of cell death in ADA2$^{-/-}$ U-937 cells at baseline and after induction of apoptosis and necroptosis *in vitro*. (A) Cell death in U-937 cells was measured by flow cytometric measurement after staining with Annexin V and Zombie® viability dye. Cells were incubated for 5 hours. Apoptosis and necroptosis were induced by stimulation with 100 nM birinapant (SM) ± 20 μM Z-VAD-FMK (Z-VAD) followed by 20 ng/mL TNF-α. Inhibition of necroptosis was achieved by adding 10 μM necrostatin-1s (Nec-1s). The experiment was performed for n = 5 distinct ADA2$^{-/-}$ U-937 cell clones. (B) Induction of apoptosis and necroptosis in U-937 cells by western blot. Whole cell lysates were produced after 5-hour incubation as for A. The plots show protein levels from n=5 independent experiments. All blots are depicted in **Supplementary Figure S2C**. (C) Cell death in lymphocytes from healthy controls (HC) and DADA2 patients was measured by flow cytometry after staining with Annexin V and Zombie® viability dye after 48-hour incubation *in vitro*. Data from n = 9 (HC) and n = 8 (DADA2, comprising n = 7 distinct patients) independent experiments are shown. The median is indicated in all plots. Mann-Whitney-U test, *p < 0.05. The patients' phenotype is indicated by colour as displayed in **Figure 1B**.

Legend: CC3, cleaved caspase-3; MLKL, mixed lineage kinase domain like pseudokinase; Nec-1s, necrostatin-1s; SM, Smac mimetic; Z-VAD, Z-VAD-FMK.

Figure 4: Analysis of cell death in DADA2 after inhibition of regulated cell death pathways. Cell death was measured by flow cytometric measurement of staining with Annexin V and Zombie® viability dye. Apoptosis, necroptosis and pyroptosis were inhibited by incubation with 20 μM Z-VAD-FMK (Z-VAD), 10 μM necrostatin-1s (Nec-1s) and 20 μM Z-YVAD-FMK (Z-YVAD), respectively, for the indicated periods of time. (A) Data from n = 12|12|8 (HC) and n = 8|8|5 (DADA2) independent experiments for Z-VAD|Nec-1s|Z-YVAD, respectively, are shown. (B) The experiment was performed for n = 2 distinct ADA2$^{-/-}$ U-937 cell clones. (C) Data from n = 5 (HC) and n = 4 (DADA2) independent experiments are shown. (D) Ferroptosis was inhibited by 48-hour incubation with 50 μM deferoxamine (DFO) or 2 μM ferrostatin-1 (Fer-1) in n = 2 HC and DADA2 patients. The median is indicated in all plots. Mann-Whitney-U test, *$p < 0.05$, **$p < 0.01$. The patients' phenotype is indicated by colour as displayed in **Figure 1B**.

Figure 5: Cell death in DADA2 upon inhibition of inflammatory pathways. Cell death was measured by flow cytometric measurement of staining with Annexin V and Zombie® viability dye in (A) U-937 cells and (B) lymphocytes after incubation with 5 μg/mL adalimumab (ADM), 5 μM ruxolitinib (Rux) or 1 μM H-151 for the indicated periods of time. (C) Gene expression of the interferon stimulated genes *IFI27* and *RSAD2* was determined by qPCR in ADA2$^{WT/WT}$ and ADA2$^{-/-}$ U-937 cells. The experiment was performed for n = 5 distinct ADA2$^{-/-}$ U-937 cell clones measured at multiple time points. mRNA expression was normalized to *HPRT1* and is depicted relative to the WT-expressing cells (RQ). (D) PBMCs from two healthy controls were incubated with supernatant of PBMCs from healthy controls (HC) (n=6) and DADA2 patients (n=6) for 48 hours. Cell death was

measured by flow cytometric measurement of staining with Annexin V and Zombie® viability dye. (E) Cell death in lymphocytes from healthy controls (HC) and DADA2 patients was measured by flow cytometry after 48-hour incubation with supernatant of HEK293T cells overexpressing the indicated *ADA2* variants. Cell death was determined by staining with Annexin V and Zombie® viability dye. (F) Cell death in $ADA2^{WT/WT}$ and $ADA2^{-/-}$ U-937 cells was measured by flow cytometry after transduction with empty vector or WT *ADA2* to restore ADA2 protein expression (**Supplementary Figure S4**). Significance is depicted as compared to cell death levels of $ADA2^{WT/WT}$ cells transduced with EV. All plots show median and 25^{th} and 75^{th} percentiles where applicable. Mann-Whitney-U test, $*p < 0.05$, $**p < 0.01$, $****p < 0.0001$. The patients' phenotype is indicated by colour as displayed in **Figure 1B**.

Legend: EV, empty vector; WT, wild type.

Figure 6: Proliferation and morphology of ADA2-deficient cells. (A) CellTrace™ Proliferation Assay was performed in $ADA2^{WT/WT}$ and $ADA2^{-/-}$ U-937 cells over 4 days. Cells were prepared for flow cytometry at baseline and after 2 and 4 days of incubation. (B) Cell death of $ADA2^{WT/WT}$ and four different clones of $ADA2^{-/-}$ U-937 cells was measured by flow cytometry during the incubation of the CellTrace™ Proliferation Assay. Dead cells were identified as Annexin V / Zombie® double-positive cells. (C) Immunofluorescence microscopy of $ADA2^{WT/WT}$ and $ADA2^{-/-}$ U-937 cells stained for ADA2. DAPI was used for nuclear staining. The scale bar represents 50 μm.

Figure 7: Metabolomics of ADA2-deficient cells. (A) Tracer metabolomics after 24-hour incubation in RPMI medium containing ^{13}C-glucose. The analysis shows $ADA2^{WT/WT}$ (n=1) and $ADA2^{-/-}$ (n=3) U-937 cells. (B) Tracer metabolomics were performed in healthy control (HC) (n=1) and DADA2 (n=1) human monocyte-derived macrophages after 24-hour incubation in RPMI

medium containing ^{13}C-glucose. The bar graphs show the average fraction of isotopologues over the three replicates. The x-axis indicates the number of labelled C atoms in the respective molecule.

Figure 8: Pentose phosphate pathway and oxidative stress in DADA2. (A) Analysis of gene expression by single-cell RNA sequencing in HC and DADA2 monocytes based on the data published by Watanabe et al (GSE142444).[11] Heatmap showing the normalized log reads (z-scores) of the genes associated with the pentose phosphate pathway (reactome id R-HSA-71336). Of these, *PGD* and *RBKS* show a significant difference at logFC=-0.37, FDR=0.03 and logFC=-2.35, FDR=0.02 respectively. (B) Schematic overview of the reactions of the pentose phosphate pathway. (C) Total content of reactive oxygen species was measured by flow cytometry in ADA2$^{WT/WT}$ and ADA2$^{-/-}$ Jurkat cells at baseline and after incubation with H_2O_2. (D) Total content of reactive oxygen species was measured by flow cytometry in PBMCs from healthy controls (HC) and DADA2 patients P5 and P6 at baseline and after incubation with H_2O_2. P6 had undergone successful HSCT at the time of sampling.

Legend: 6PGD, 6-phosphogluconate dehydrogenase; 6PGL, 6-phosphogluconolactonase; G6PD, glucose-6-phosphate dehydrogenase; gMFI, geometric mean fluorescence intensity; ROS, reactive oxygen species.

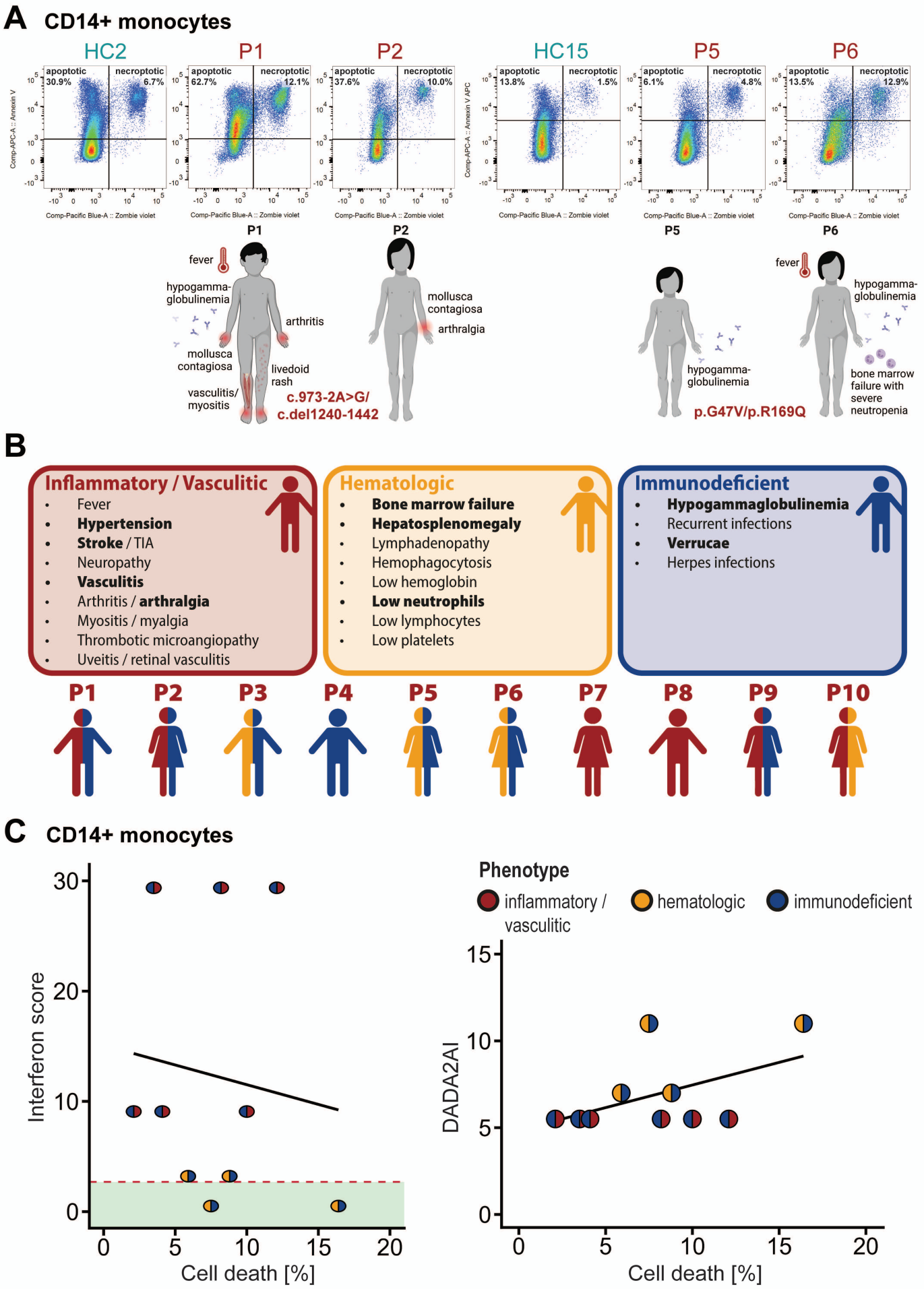
A
CD14+ monocytes
HC2
P1
P2
HC15
P5
P6
apoptotic
necroptotic
30.9%
6.7%
62.7%
12.1%
37.6%
10.0%
13.8%
1.5%
6.1%
4.8%
13.5%
12.9%
Comp-APC-A :: Annexin V
Comp-Pacific Blue-A :: Zombie violet
P1
fever
hypogamma-globulinemia
arthritis
mollusca contagiosa
livedoid rash
vasculitis/ myositis
c.973-2A>G/ c.del1240-1442
P2
mollusca contagiosa
arthralgia
P5
hypogamma-globulinemia
p.G47V/p.R169Q
P6
fever
hypogamma-globulinemia
bone marrow failure with severe neutropenia
B
Inflammatory / Vasculitic
Fever
Hypertension
Stroke / TIA
Neuropathy
Vasculitis
Arthritis / arthralgia
Myositis / myalgia
Thrombotic microangiopathy
Uveitis / retinal vasculitis
Hematologic
Bone marrow failure
Hepatosplenomegaly
Lymphadenopathy
Hemophagocytosis
Low hemoglobin
Low neutrophils
Low lymphocytes
Low platelets
Immunodeficient
Hypogammaglobulinemia
Recurrent infections
Verrucae
Herpes infections
P1
P2
P3
P4
P5
P6
P7
P8
P9
P10
C
CD14+ monocytes
Interferon score
Cell death [%]
Phenotype
inflammatory / vasculitic
hematologic
immunodeficient
DADA2AI
Cell death [%]

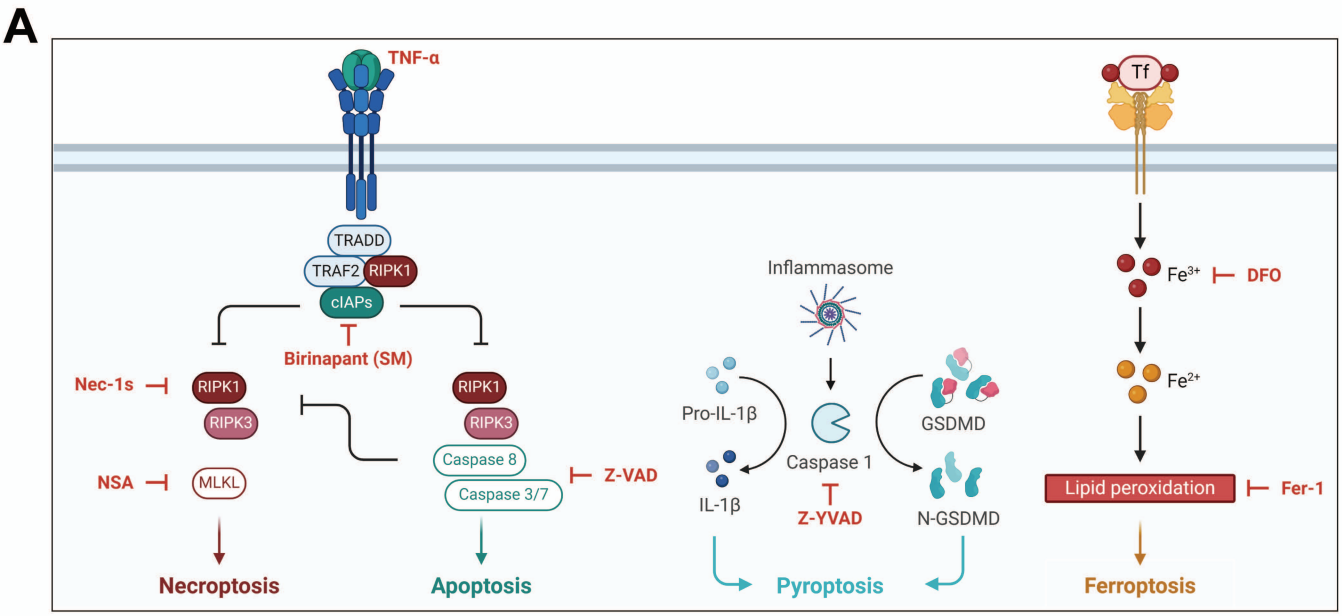
A
TNF-α
TRADD
TRAF2
RIPK1
cIAPs
Birinapant (SM)
Nec-1s
RIPK1
RIPK3
NSA
MLKL
Necroptosis
RIPK1
RIPK3
Caspase 8
Caspase 3/7
Z-VAD
Apoptosis
Inflammasome
Pro-IL-1β
IL-1β
Caspase 1
Z-YVAD
GSDMD
N-GSDMD
Pyroptosis
Tf
Fe3+
DFO
Fe2+
Lipid peroxidation
Fer-1
Ferroptosis

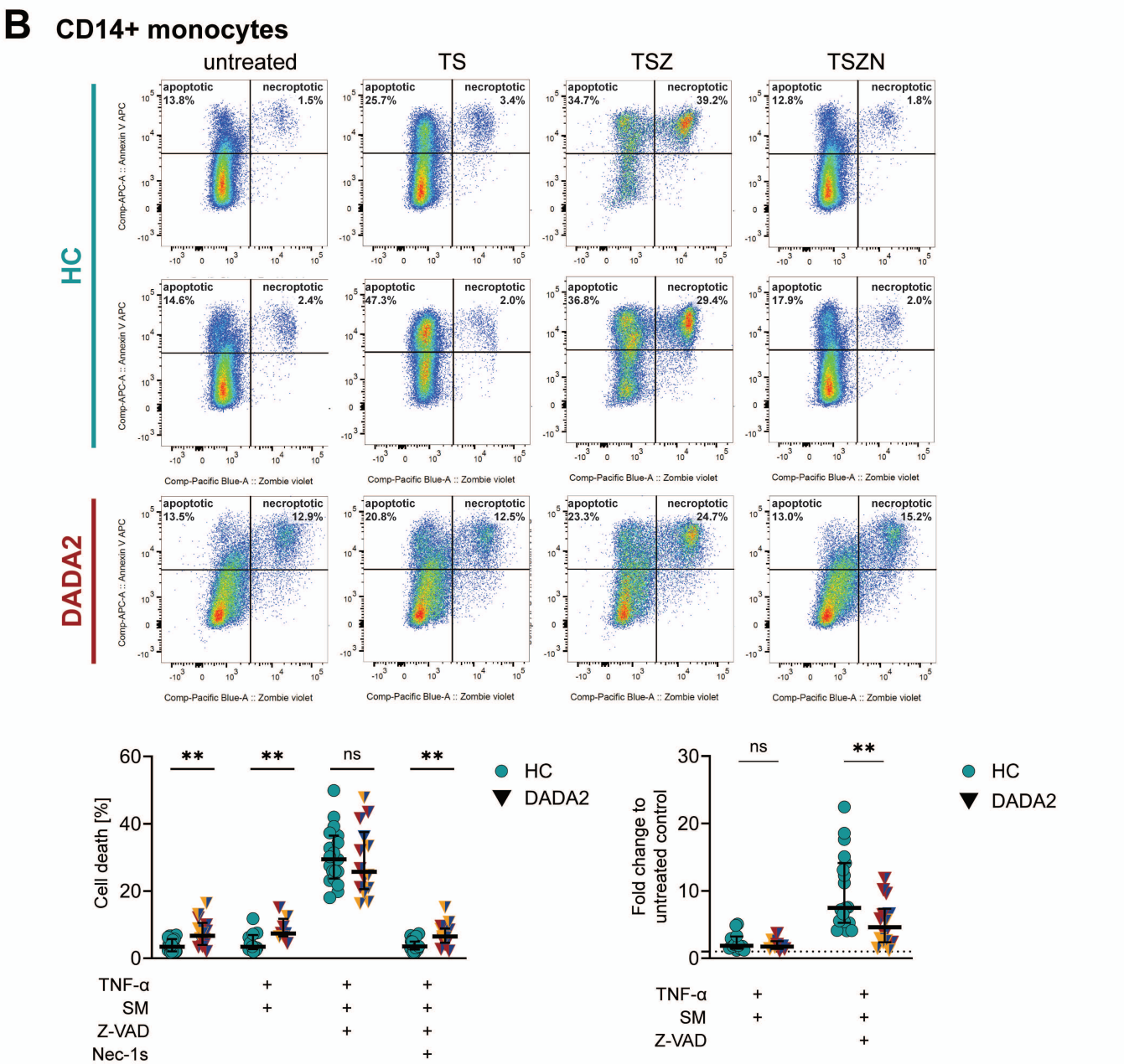
B
CD14+ monocytes
untreated
TS
TSZ
TSZN
HC
DADA2
apoptotic
necroptotic
13.8%
1.5%
25.7%
3.4%
34.7%
39.2%
12.8%
1.8%
14.6%
2.4%
47.3%
2.0%
36.8%
29.4%
17.9%
2.0%
13.5%
12.9%
20.8%
12.5%
23.3%
24.7%
13.0%
15.2%
Comp-APC-A :: Annexin V APC
Comp-Pacific Blue-A :: Zombie violet
Cell death [%]
Fold change to untreated control
HC
DADA2
ns
**
TNF-α
SM
Z-VAD
Nec-1s

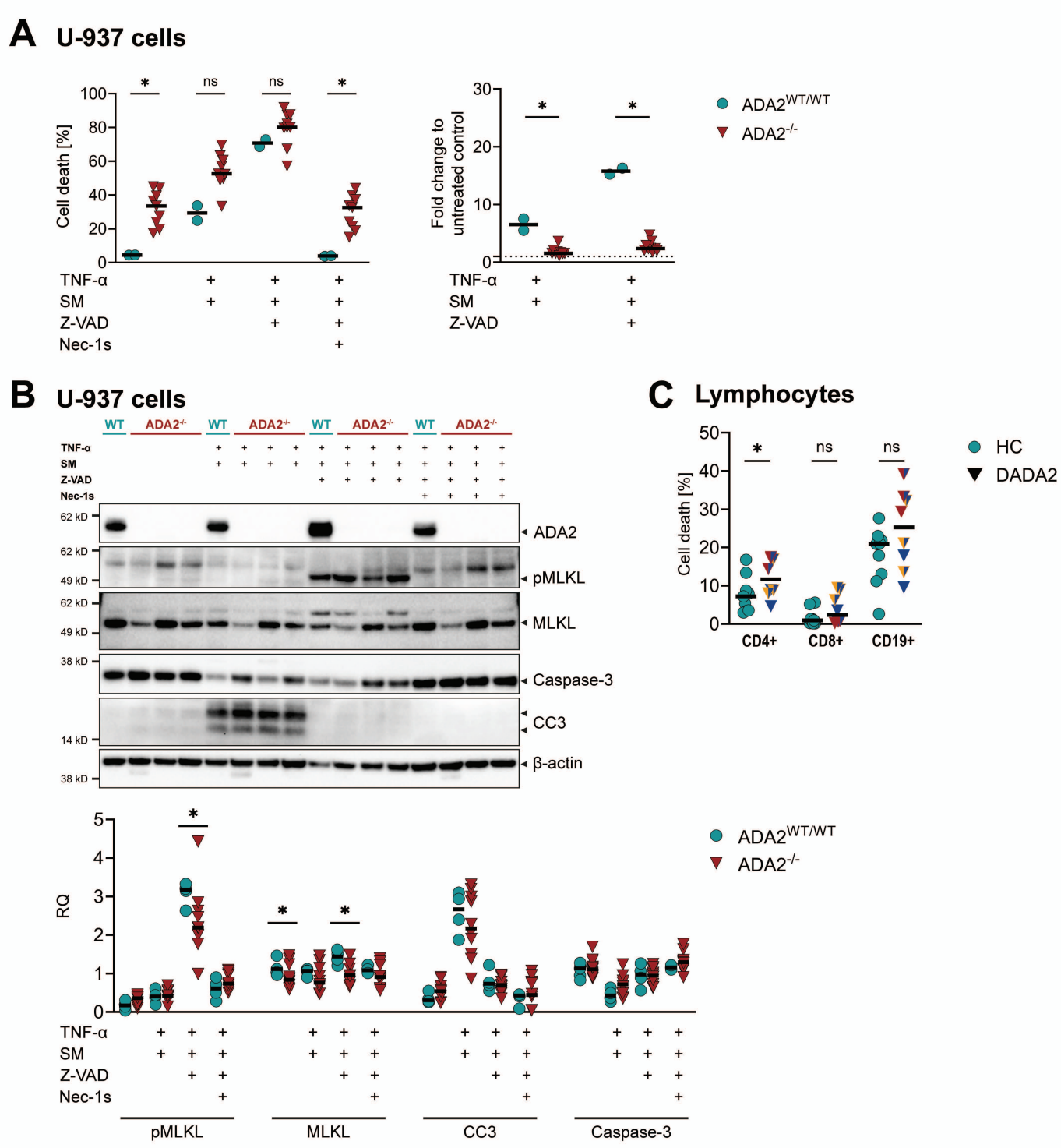
A
U-937 cells
Cell death [%]
100
80
60
40
20
0
*
ns
ns
*
TNF-α
SM
Z-VAD
Nec-1s
Fold change to untreated control
30
20
10
0
*
*
ADA2WT/WT
ADA2-/-
B
U-937 cells
WT
ADA2-/-
WT
ADA2-/-
WT
ADA2-/-
WT
ADA2-/-
TNF-α
SM
Z-VAD
Nec-1s
62 kD
ADA2
62 kD
49 kD
pMLKL
62 kD
49 kD
MLKL
38 kD
Caspase-3
CC3
14 kD
38 kD
β-actin
RQ
5
4
3
2
1
0
*
*
*
ADA2WT/WT
ADA2-/-
TNF-α
SM
Z-VAD
Nec-1s
pMLKL
MLKL
CC3
Caspase-3
C
Lymphocytes
Cell death [%]
50
40
30
20
10
0
*
ns
ns
CD4+
CD8+
CD19+
HC
DADA2

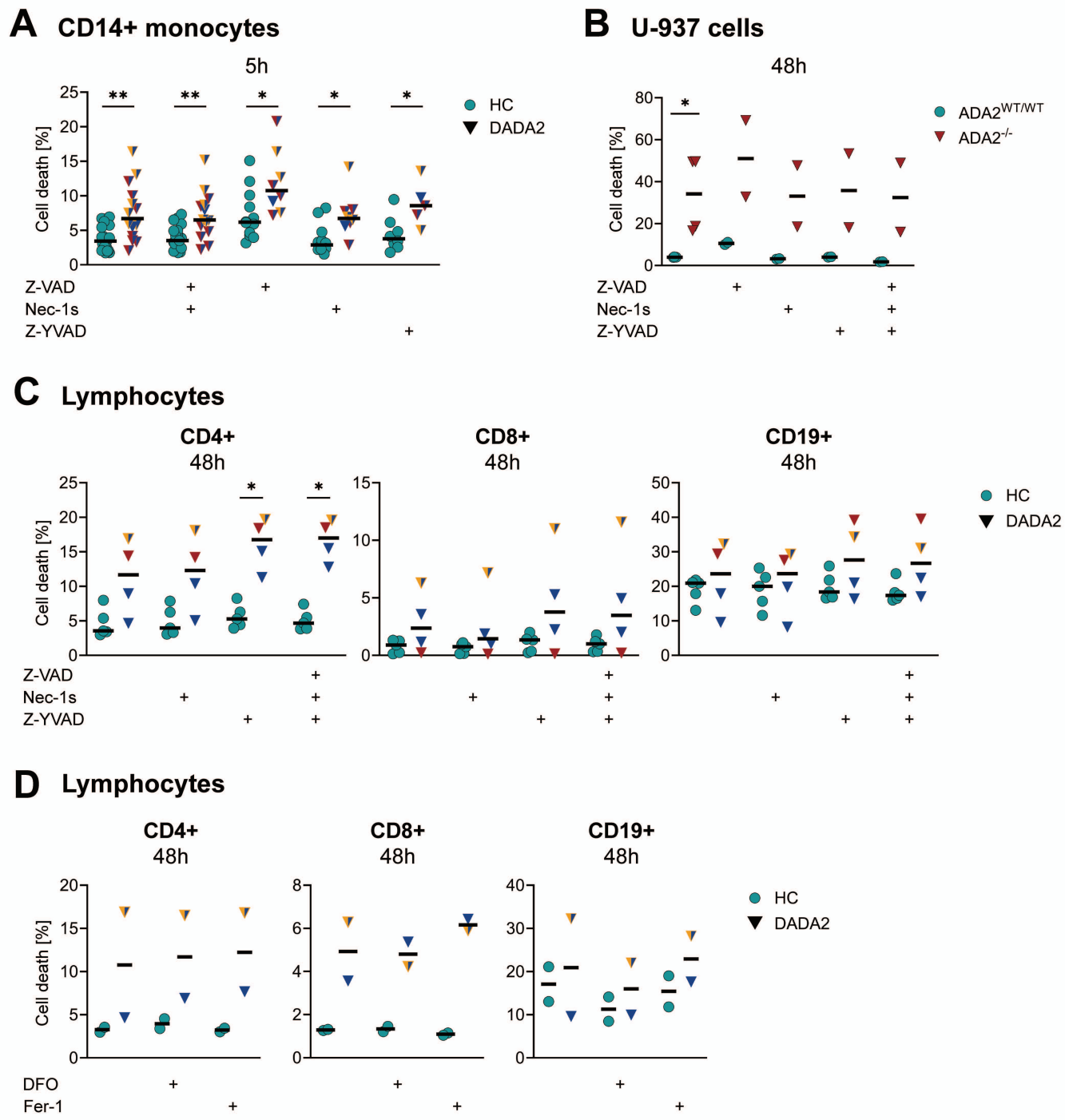
A
CD14+ monocytes
5h
Cell death [%]
HC
DADA2
Z-VAD
Nec-1s
Z-YVAD
B
U-937 cells
48h
ADA2WT/WT
ADA2-/-
C
Lymphocytes
CD4+
48h
CD8+
48h
CD19+
48h
D
DFO
Fer-1

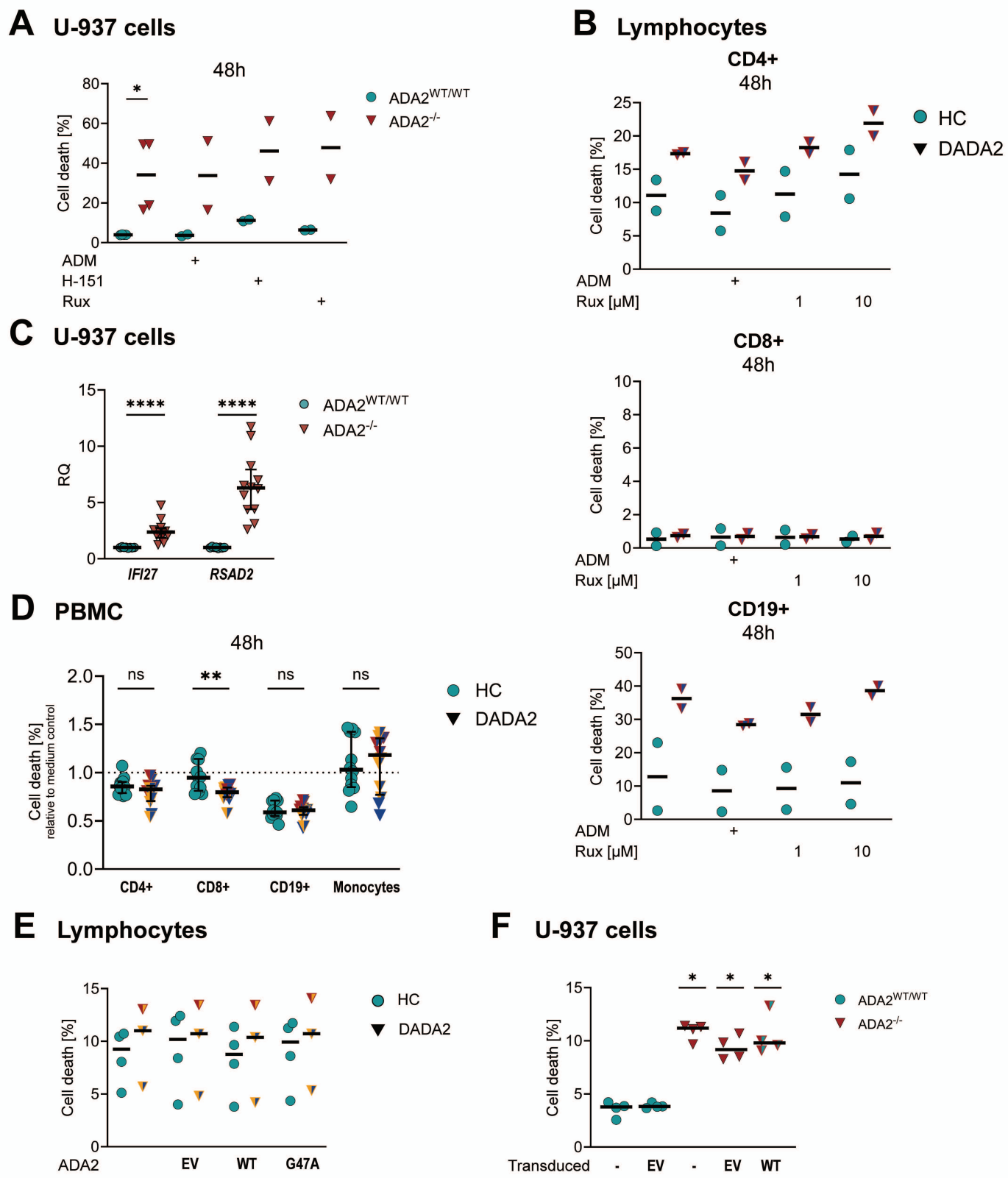
A
U-937 cells
48h
Cell death [%]
ADA2WT/WT
ADA2-/-
ADM
H-151
Rux
B
Lymphocytes
CD4+
48h
HC
DADA2
Rux [μM]
CD8+
CD19+
C
U-937 cells
RQ
IFI27
RSAD2
D
PBMC
Cell death [%] relative to medium control
CD4+
CD8+
CD19+
Monocytes
E
Lymphocytes
ADA2
EV
WT
G47A
F
U-937 cells
Transduced

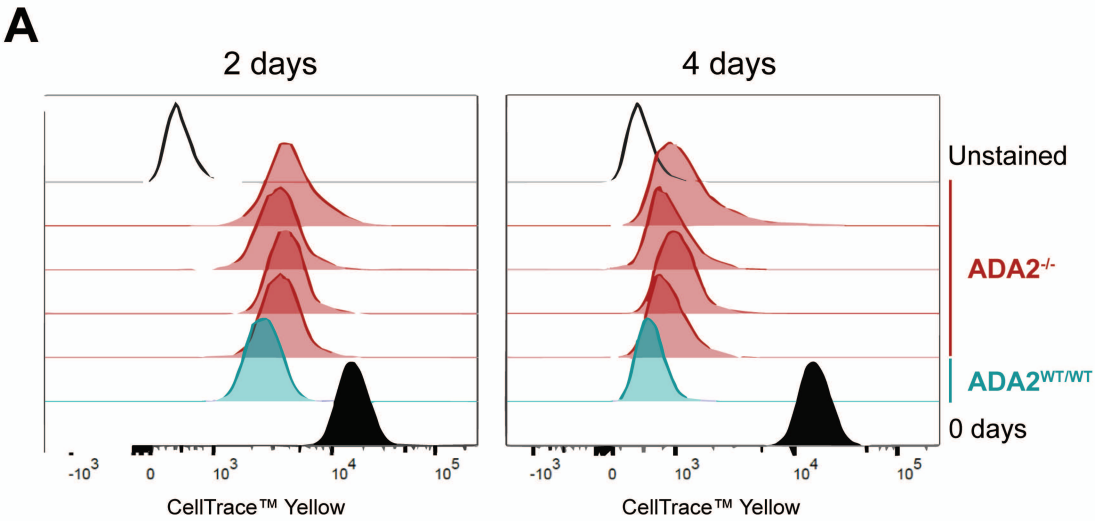
A
2 days
4 days
Unstained
ADA2-/-
ADA2WT/WT
0 days
-10^3
0
10^3
10^4
10^5
CellTrace™ Yellow
CellTrace™ Yellow

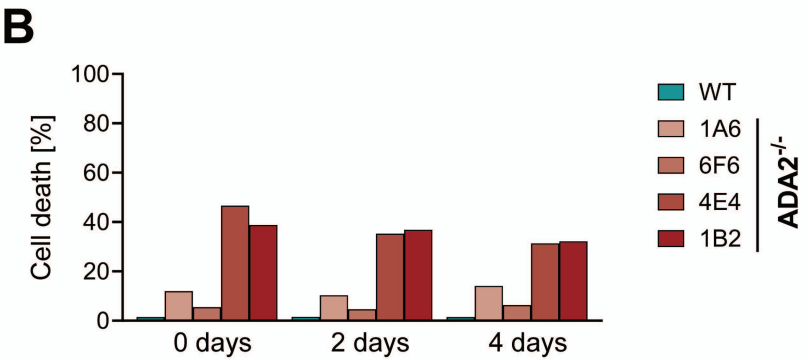
B
Cell death [%]
100
80
60
40
20
0
0 days
2 days
4 days
WT
1A6
6F6
4E4
1B2
ADA2-/-

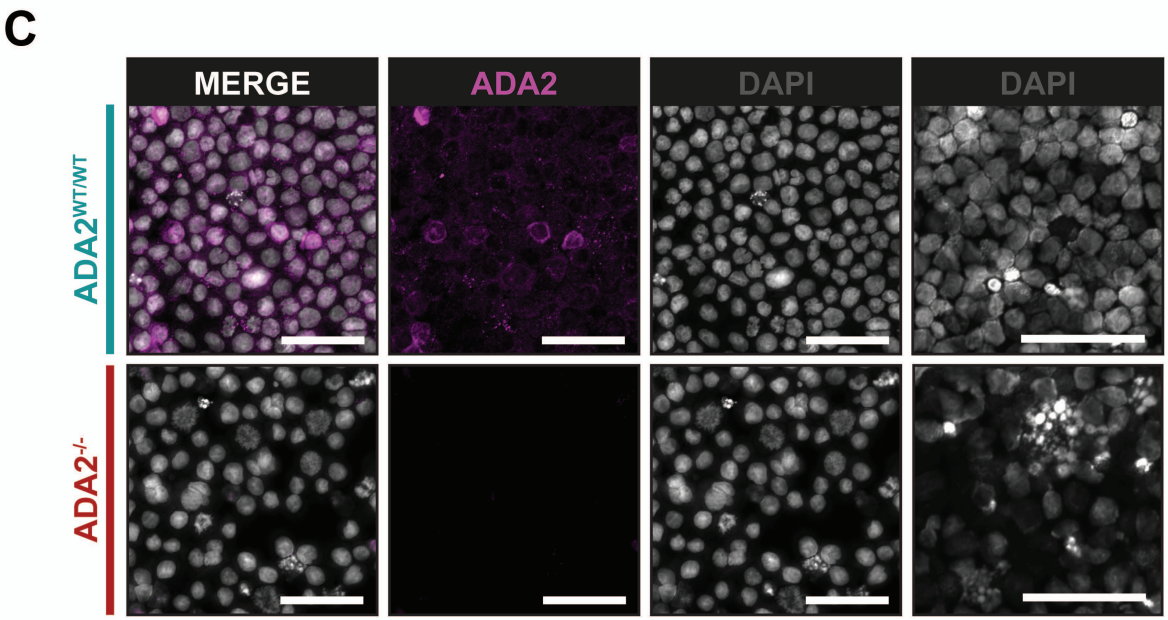
C
MERGE
ADA2
DAPI
DAPI
ADA2WT/WT
ADA2-/-

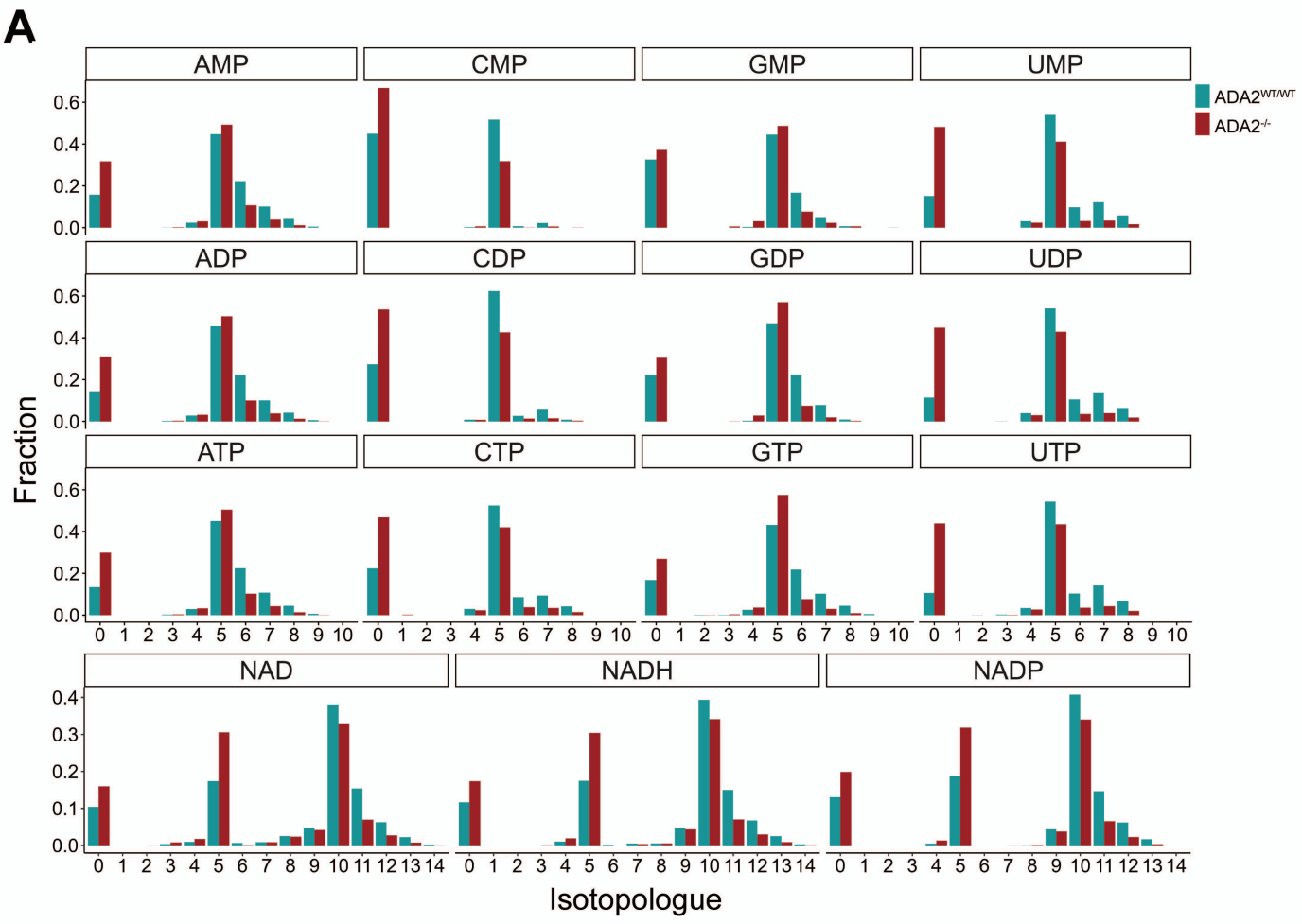
A
AMP
CMP
GMP
UMP
ADP
CDP
GDP
UDP
ATP
CTP
GTP
UTP
NAD
NADH
NADP
ADA2WT/WT
ADA2-/-
Fraction
Isotopologue

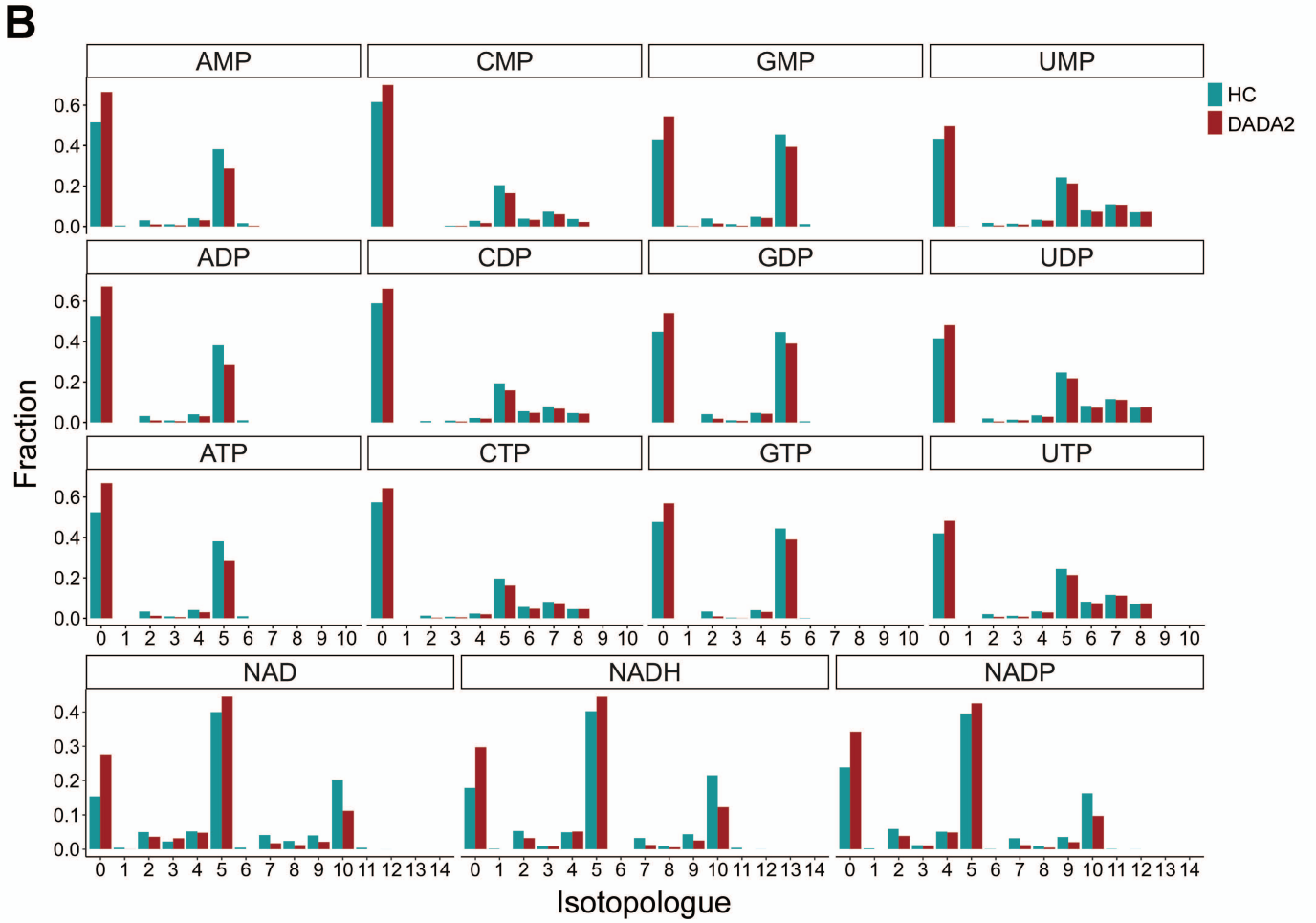
B
AMP
CMP
GMP
UMP
ADP
CDP
GDP
UDP
ATP
CTP
GTP
UTP
NAD
NADH
NADP
HC
DADA2
Fraction
Isotopologue

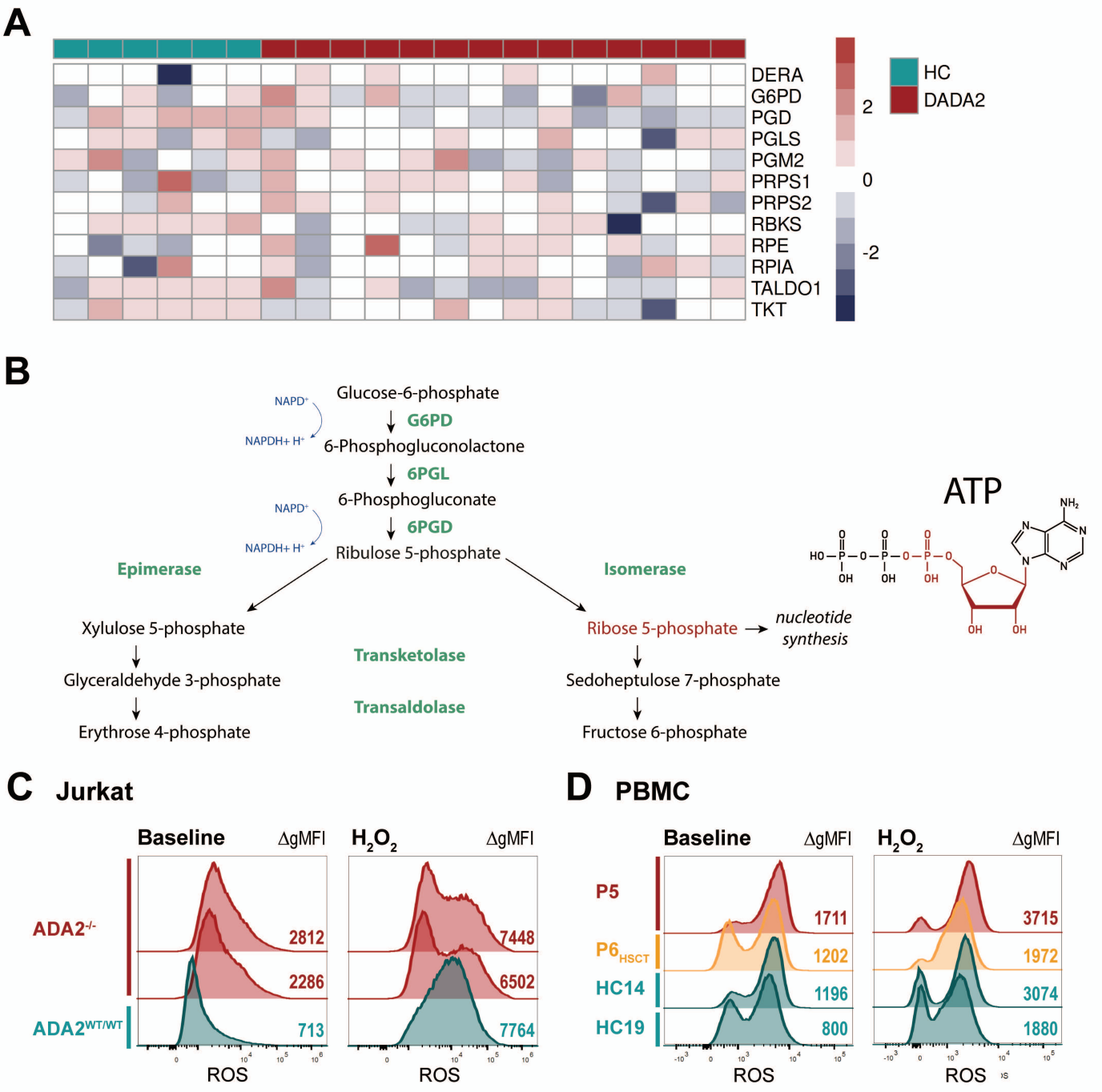
A
DERA
G6PD
PGD
PGLS
PGM2
PRPS1
PRPS2
RBKS
RPE
RPIA
TALDO1
TKT
2
0
-2
HC
DADA2
B
Glucose-6-phosphate
NAPD+
NAPDH+ H+
G6PD
6-Phosphogluconolactone
6PGL
6-Phosphogluconate
NAPD+
NAPDH+ H+
6PGD
Ribulose 5-phosphate
Epimerase
Isomerase
Xylulose 5-phosphate
Glyceraldehyde 3-phosphate
Erythrose 4-phosphate
Transketolase
Transaldolase
Ribose 5-phosphate
nucleotide synthesis
Sedoheptulose 7-phosphate
Fructose 6-phosphate
ATP
C Jurkat
Baseline
ΔgMFI
H2O2
ΔgMFI
ADA2-/-
ADA2WT/WT
2812
2286
713
7448
6502
7764
ROS
ROS
D PBMC
Baseline
ΔgMFI
H2O2
ΔgMFI
P5
P6HSCT
HC14
HC19
1711
1202
1196
800
3715
1972
3074
1880
ROS
ROS